ISLAMIC AZAD UNIVERSITY

SOUTH THEHRAN BRANCH

FACULTY OF TECHNICAL AND ENGINEERING

DEPARTMENT OF ENERGY SYSTEMS ENGINEERING

"M.Sc." THESIS

SUBJECT:

THE SIMULATION OF ORGANIC SOLAR CELLS AND ITS COMPARISON TO EXPERIMENTAL RESULTS

THESIS ADVISOR:
KAMAL ABBASPOUR SANI, Ph.D.

CONSULTING ADVISOR:
PARISHA FIROUZIAN, Ph.D.

BY:
MAHLA SHARIATZADEH

JAN 2016

دانشگاه آزاد اسلامی

واحد تهران جنوب

دانشکده فنی و مهندسی

پایان نامه برای دریافت درجه کارشناسی ارشد *"M.Sc."*

مهندسی سیستم های انرژی – سیستم های انرژی

عنوان :

شبیه سازی سلول های خورشیدی آلی و مقایسه آن با نتایج تجربی

نگارش:

مهلا شریعت زاده

امضاء هیأت داوران پروژه:

استاد راهنما: دکتر کمال عباسپورتانی

استاد مشاور: دکتر پریشا فیروزیان

هیأت ژوری: دکتر فریور فاضلپور

هیأت ژوری: دکتر کوروش امیر اصلانی

مدیر گروه: دکتر حسین احمدی دانش

تاریخ دفاعیه: ۱۴/ ۱۰/ ۱۳۹۴

Table of Contents

List of tables

Title

List of figures

Title

List of charts

Title

Abstract

The simulation of bulk heterojunction organic solar cell was performed by Comsol Multiphysics software which was consistently described by the voltage- current and voltage- power characteristics (electric characteristics). In this study, we compared the experimental data to simulation one of the OC1C10PPV:PCBM (poly[2-methoxy-5-(3'7'-dimethyloctyloxy)-p-phenylene vinylene]: (6,6)-phenylC61-butyric acid methylester) for the validation and verification of software results and performance initially. Then the simulation of other components for P3HT:PCBM (poly(3-hexylthiophene) and PCPDTBT:PCBM (poly[2,6-(4,4-bis-(2-ethylhexyl)-4H-cyclo-penta[2,1-b;3,4-b0]dithiophene)-alt-4,7-(2,1,3-benzothiadiazole) were studied. As assumption the parameters such as temperature and electron affinity were constant, the power conversion efficiency, external quantum efficiency, fill factor, Voc, Jsc, and current changes along with the active layer thickness were studied. The simulation results predicted the power conversion efficiency for OC1C10PPV:PCBM and P3HT:PCBM is 2.7% and 5% respectively, which is indicated the reliability of simulation for organic solar cells.

Chapter One

Introduction

Introduction

Not only is the sun a great source of energy, it is the beginning of life and the source of all other energies. According to scientific estimates, about 6,000 million years have passed since the birth of this fiery orb, and 4.2 million tons of sunlight are converted into energy every second. Given the weight of the sun, which is about 333,000 times the weight of the Earth. This luminous globe can be a huge source of energy for the next 5 billion years.

The diameter of the sun is 1.39 * 106 km and about 99% of the sun's weight is made up of hydrogen and helium gases, about 70% hydrogen, 29% helium, and the rest 1%, including 63 other elements, most notably oxygen, carbon, neon and nitrogen. Is formed. The temperature in the center of the sun is about 10 to 14 million degrees Celsius, which emits from the surface at a temperature of about 5600 degrees in the form of electromagnetic waves in space. The Earth is about 150 million kilometers from the sun, and it takes 8 minutes and 18 seconds for the sun to reach the earth, so the Earth's share of the sun's energy is about 109 * 2 1/2 of its total radiant energy.

Fossil fuels stored deep within the earth, wind and waterfall, and waves of the seas and many more are the results of the same amount of low energy received from the sun. [26]

Today, human resources are supplied by a variety of sources, most of which are fossil fuels such as oil, coal and natural gas. Therefore, the diversification of renewable energy sources is necessary to reduce CO2 emissions, methane and other harmful substances. The sun is one of the sources of free, clean and free of harmful environmental effects that has been used by humans in a variety of ways. In recent years, the use of this energy source has led to the emergence of energy converters and solar cells. A solar cell is a device that converts solar energy by means of a photovoltaic effect (direct conversion of solar energy into electricity) without connecting it to an external voltage source [1].

In the late 1950s, solar cells were used to power the satellite systems because they did not require maintenance for a long period of time, and without much loss in conversion efficiency, They were very helpful. In the 1970s, scientists found that using the photovoltaic effect could be a good proposition to generate energy from non-fossil sources [2]. For the past century, the economy has focused on various sources of energy such as nuclear, water, wind, oil and gas. Electricity generation using coal, gas, and oil emits large amounts of pollution (carbon dioxide), and therefore health risks. Nuclear energy is very expensive and involved in the issue of radiation and hazardous waste. All of these sources of electricity are involved in day-to-day maintenance, transportation and delivery despite adverse weather conditions. Solar energy, on the other hand, provides a source of pollution-free, unnecessary transportation aids. Despite these benefits, solar cells generate only 0.04% of the world's electricity, which is due to the high cost of producing these cells [2].

Among the applications of the cells of grace are the following: [3]:

• Supply motors of satellites and spaceships

• Power supplies for devices that require low voltages (such as calculators and clocks)

• Provision of city electricity by photovoltaic power plants

• Providing the necessary force for moving cars and small boats

Various materials have so far been used in the manufacture of solar cells that have different manufacturing efficiencies and costs. In fact, these cells must be designed to convert the wavelengths of sunlight that reach the surface of the Earth to high energy efficiency. The materials used to make solar cells fall into four generations, according to Table 1.

Table1-1 -Examine the Types, Disadvantages, and Benefits of Solar Cells

Disadvantages	Advantages	Compounds of constituent)Types(	Solar Cells
• High Costs :High cost production technologies such as) : a (silicon extraction from sand and purification before crystal growth; (b (high energy consumption when growing and cutting ingots. • The highest amount of energy photons are wasted at the blue and violet end of the heat wave • Energy consumption as fossil fuels	• Wide absorption spectrum range (1.12ev) • High fluidity of carrier	Single crystalline silicon wafers	First generation
• Lower efficiency than first generation silicon wafers • Inherent violations due to lower quality of control method • Amorphous silicon instability • High toxicity	• Low production cost • Requires fewer materials because of the low cost-to-power) W (ratio and also the lightweight • Flexibility and its effect on matching panels on curved surfaces or lightweight flexible materials such as fabrics • Tubing capability	• Silicone-free • Polycrystalline silicon • Cadmium telluride • Indium Gallium Di Selenide Copper Alloy	Second generation

Disadvantages	Advantages	Compounds of constituent)Types(	Solar Cells
• Low efficiency compared to silicon wafers • Polymeric Solar Cells, Degradability and Performance Reduction Over Time Due to Environmental Impacts, High Energy Gap • Electrolyte Destruction of Electrodes in Photoelectrochemical Cells	• Low energy technologies for mass production • The ability of polymer cells to be controlled in terms of chemical synthesis and low cost of synthesis • Working in low light conditions, with color sensitized solar cells being rechargeable and rechargeable	• Nanocrystalline cells • Photoelectrochemical cells • Polymer cells • Color-Sensitive Solar Cells	third generation
• Lower efficiency than silicon wafers • Degradable like polymer cells • Optimization of conductive polymers and nanocrystals	• Solubility control • Low Cost Materials) Polymers(• Khvdchydmany) assembly(• Printable nanocrystals on the polymer layer • Improved energy conversion efficiency	• Hybrid mineral crystals inside the polymer matrix	The fourth generation

Problem Statement

Solar cells are manufactured in a variety of technologies, including organic solar cells, and are one of the newest techniques in manufacturing. These types of cells have attracted a great deal of attention because of their advantages such as easy processing, flexibility, light weight and low manufacturing cost. In this research, solar cells are based on organic matter that is part of the third generation of solar cells. The most important components of organic solar cells are the donor and acceptor, which are the most important components to conductive polymers such as Poly [2-

methoxy-5- (2-ethylhexyloxy) -1,4- phenylenevinylene] (MEH-PPV) and P3HT (poly (3-hexylthiophene)) and of the receptor materials to the fullerene derivatives. Among the different methods of bonding in solar cells, the Bulk Heterojunction Solar Cells (BHJ) method is one of the best ways to increase the level of contact and donor and facilitate electron transfer.

Organic solar cells have various types, most notably color-sensitive solar cells, polymer solar cells, and liquid crystal-based solar cells.

The author intends to study solar organic cells, especially polymer. Based on Conjugated Polymers based polymer solar cell work, these polymers have recently been used for their applications in flexible electronic devices such as light emitting diodes (LEDs), polymer solar cells and organic thin-film transistors. Processing in solution and their low cost have received special attention.

The thickness of the active layer in organic polymer solar cells is 100nm, which is approximately 1000 times thinner than crystalline silicon solar cells and 10 times thinner than inorganic films.

However, this type of solar cell is 2 to 3 times less efficient than mineral cells. For this reason, many semiconductor materials have been developed to enhance and enhance the functionality of these polymer cells, but scientists are working hard to make the ideal material in this field.

Purpose and innovation

In this study, using different techniques mentioned in the implementation method, the results of changing the organic thickness of polymer with different thicknesses with respect to open voltage (voc) and short-circuit current density (Jsc) in the performance of common solar cells It is investigated as well as the power efficiency (PCE) and external quantum efficiency (EQE) due to the change of different active layer materials. In this way, the optimal model of the solar cell will be obtained with suitable material and thickness of choice. As noted, scientists have been working hard to build a solar cell with various ideal materials to maximize the efficiency of this type of cell, and the ultimate goal of the thesis is to innovate and obtain an optimal model. Also check the reliability of the software used (COMSOL) to perform this simulation.

Background

The history of using the polymer technique in solar cells goes back to 1977, when the first conductive semiconductor polymers were developed by Chiang et al. (1977). He and his colleagues showed that polyacetylene semiconductor polymer films show a significant increase in electrical conductivity when impregnated with controlled amounts of arsenic pentafuoride with halogens chlorine. Subsequently, as the technology progressed, organic molecules and semiconductor polymers were increasingly used in optical electronics. In fact, because of the small molecules of these cells, they make solar cells much lighter and less expensive.

With the integration of organic and inorganic composites, a unique path was created in the design of solar cells. This process continued until 1986 by Tang Tang by incorporating tetracarboxylic

perylene organic matter (PV) and a layer of copper phthalocyanine derivatives (CuPc))) as donor and receptor The first positive and negative structure in donor and receptor components was created under the AM2 simulation conditions. Although the cell yield was about 1%, it was the beginning of a new chapter in the design of these cell types.

In 2008, research by Peumans and Hadipour (Peumans et al. 2003 and Hadipour et al. 2008) showed that widespread changes in the structure of ingredients in organic polymer and the use of tandem materials and changes in cell architecture yielded Increased by more than 6%. He and his colleagues showed that in order to obtain more efficient organic solar cells, the narrowest optical absorption of the active layer had to be modified using two or more donor materials, without overlapping the absorption spectrum in a tandem or hybrid structure so that all Absorb the sun's visible area and even near the infrared range. As a result, it plays an important role in the different structures of the bilayer cells that separate the two subcells. He showed that the final efficiency depends directly on the electrical properties (ohmic bonding and proper conductivity) and the optical properties (transparency) of the middle electrode.

Method of doing research

In this thesis, the preliminary data, which are the same research variables and materials with different thicknesses, are selected and can be used with various techniques such as algorithm (FDTD) in the mathlab environment and related simulation software such as Fluxim, COMSOL multiphysics, Silvaco Atlas , Setfos, various simulation materials performed herein Selected by COMSOL. As a result, this polymer solar cell simulation is investigated as a heterogeneous connection. The results of the organic-polymer change with respect to the open voltage (voc) and short-circuit current density (Jsc) are investigated, as well as the efficiency (PCE) and external quantum efficiency (EQE) as well as the changes of the current due to the change The thickness of the active layer of the various materials is studied to obtain the optimal model of the solar cell with the appropriate material. The constructs are compared with the results in empirically determined research literature.

Organic Solar Cell Components and the Function of Polymer Solar Cells

Common components of organic solar cells are as follows:

•Glass

• Transparent conductive material such as (Indium-Tin Oxide, ITO)

Conductive transparent polymer (organic HTL donor) such as PEDOT: PSS

• Active layer (organic ETL acceptor)

• Connecting layer

• Metal (together with the cathode bonding layer)

Figure 1-1: Organic Solar Cell Components

The process of converting light into electricity by organic solar cells is schematically described as follows:

• Photon absorption, which results in an excited light state

• Production of a pair of electrons (exciton)

• Separation of charge by exciton penetration into the segregated areas

• Transfer of charge from the semiconductor to the respective electrodes [1.2]

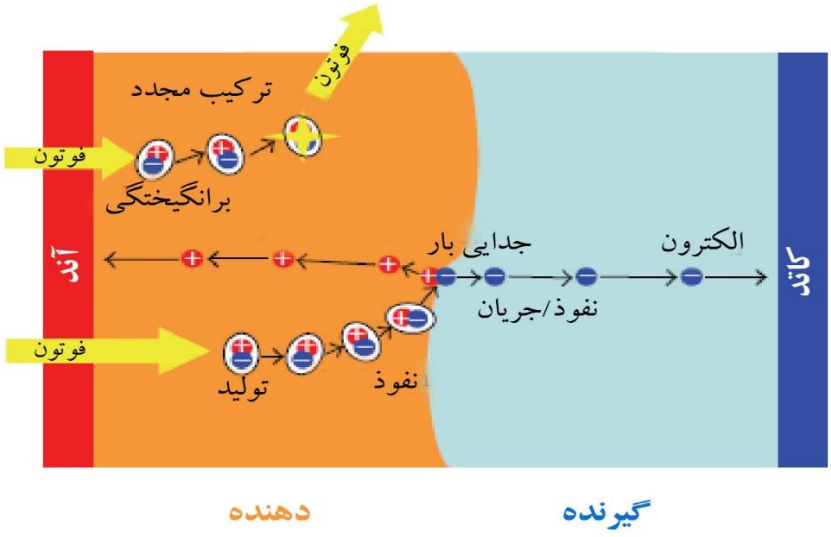

Figure 1-2: The basis of the process of converting light into electricity by organic solar cells

Chapter Two
background research

background research

The discovery of the photovoltaic effect goes back to 1839, but its development and application has been slow. With the development of quantum mechanics in the early twentieth century, it was possible to explain the phenomena of light-to-electricity conversion and the importance of single-crystal semiconductors was discovered and the behavior of n-p bonding was explained. In 1954 Chapin and his colleagues at Bell Labs invented a silicon solar cell (6% efficiency) [1].

CK Chiang and colleagues first found that semiconductor polymer films, polyacetylene, show a significant increase in their electrical conductivity when doped with arsenic penta fluride (As F5) with controlled amounts of halogens chlorine, bomine or iodine. . They also found that the use of various impurities and the replacement of the H atom in (CH) x with organic or inorganic groups lead a large new class of conducting polymers with electrical properties that can range from complete insulation to semi-insulation. Conductor to control the metal. [17]

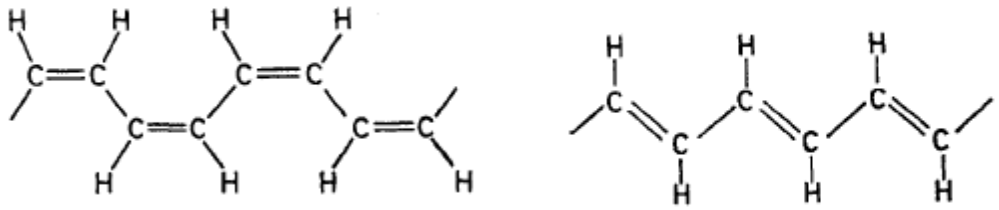

Figure 2-1

C.W Tang began his research in 1985 on a thin film, two-layer photovoltaic cell made of copper phthalocyanine derivatives and a tetracarboxylic perylene. The power conversion efficiency of about 1% was obtained under the AM2 simulation conditions. He found that its new feature, the charge generation efficiency, is relatively independent of the bias voltage. The connection line between the two organic materials is more effective in determining the photovoltaic properties than the organic / electrode contact. In this paper, the two-layer structure of organic thin films was used, which is significantly different from the conventional one-layer organic material sandwiched between two different electrodes. He also received direct bias conductivity equal to positive voltage on the ITO electrode. The I-V curve in the direct bias is derived from the Shockley relation. (Voltage between 150-550mV)

$$\left|exp\left(\frac{qv}{nkT}\right)-1\right| \qquad \text{Equation 1}$$

The highest power conversion efficiency was reported at 75mw / cm2 with no correction for reflection or absorption loss of 0.95%. And the output current has a weak dependence on the bias voltage.

He also found that the Voc of the PV / cuPc bilayer is relatively independent of the electrode material. Materials used: gold wire contact- Ag (0.1 cm2) - PV (500A0) - cuPc (300 A0) - In2o3 (300 A0) and glass. [18]

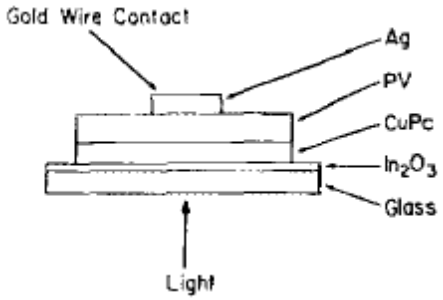

Figure 2-2 - Organic solar cell designed in the Tang model

Peumans and Forrest in their paper demonstrated that the use of a metal warhead (1000 A0 Ag) to limit organic matter during the heating process prevents the formation of a hard-core surface while forming a donor-lattice network. - Accepts the acceptor. In this method, the power conversion efficiency is up to 50% higher than the reported values for dual-layer devices. In this paper, the heating process can be performed for the formation of thin-film, high-efficiency, low-cost organic cells based on vacuum deposited small molecular weight. BHJs are also produced through the rotational coating of donor and acceptor materials. During the rotational coating process, the solvent evaporates and the donor and acceptor phases are separated, creating a complex interconnected network. Heating of completed devices has previously been used to extend the life and luminous efficiency of OLED (Organic Light Emitting Diodes) and to improve the efficiency of polymer photovoltaic cells. Although these effects are not attributable to changes in the nature of the junction line, they are attributed to the alignment of the polymer chains and the increase of the mobile charge carriers or the formation of a junction layer in the organic / cathode junction. Materials used with different thicknesses (A0): indium tin oxide (ITO) / copper phthalocyanine (CuPc) / ° CuPc: PTCBI (3: 4) / 3,4,9,10-perylene tetracarboxylic bis-benzimidazole (PTCBI). The CuPc concentration in PTCBI is 3: 4 wt. [20]

Hadi Pour and his colleagues modified the narrowest optical absorption of the active layer to obtain more efficient organic solar cells. By using two or more materials, the spectrum of sunlight can be absorbed and even extended near infrared, without overlapping the absorption spectrum in a multijunction or tandem structure. In addition, to cover a larger part of the spectrum, tandem solar cells suggest that photon energy be used more efficiently, since the voltage of the charge collected in each substrate is closer to the energy of the photons absorbed in that cell. In different tandem structures, the layer that separates both sub-cells plays an important role. The ultimate efficiency of these cells is directly related to the electrical properties (ohmic coupling and proper conductivity and conductivity) and the optical properties (transparency) of the middle electrode. Power conversion efficiency of over 6% was also reported for solution-processed organic bulk heterojunction tandem solar cells. An example of some materials used: CuPc / ZnPc / PTCBI / Me-PTC / BCP / m-MTDATA / H2Pc / C60. [21]

In their paper, Zhong and his colleagues showed that Voc and Jsc reach the maximum by optimizing energy level alignment and absorbing light from the donor and receiver. They showed that by inserting a transparent spacer insulation layer between the donor and acceptor in the organic double layer solar cells, it increased the ECT (polymer energy band gap must be related to the

absorption of light, thus maximizing Jsc gain by the cell). The energy depends on the higher occupied orbital (HOMO) of the donor and the lower unoccupied molecular orbital (LUMO) of the receiver, this difference being the EDA, which now replaces the EDA with the E CT charge transfer energy, which contains information on the structure of the D-line. / A and attenuates the charge structure of the molecule.) And prevents recombinant charge, thereby increasing Voc. Although the spacer prevents re-incorporation of charge (or charge separation), increasing the E CT factor is more important for increasing Voc. Also doping the spacer layer with one color increases Jsc by reducing energy transfer and reducing Voc.

The materials used in this study are: PCBM / CYTOP: F-SiPc // P3HT and TiO2 /PCBM/CYTOP:F-SiPc//P3HT.[22]

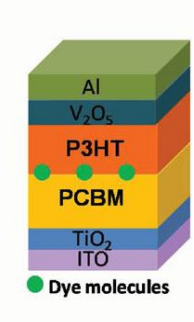

Figure 2.3 Organic solar cell designed by Zhong and his colleagues; they showed that by placing a layer of spacer on the color molecules, it increased the JSC and prevented the decrease of voc.

Jie Min and colleagues looked at the alkyl chain. To elucidate the effect of side chains, a series of star shaped molecules based on the triphenylamine (TPA) core of bithiophene and dicyanovinyl derivatives were combined with different methyl, hexyl, dodecyl alkylend-capping, ethyl groups. Alteration of the alkyl chain has a small effect on the absorption of HOMO and LUMO surfaces. All molecules have good thermal stability, similar absorption spectra in the solvent and low and similar relative HOMO levels. Design and precise control of the position and density of the different side and end chains of the blended oligomer alkyls, not only increase the solubility of the materials in the organic solvents. It also balances the band structure, which improves the photovoltaic properties. Stellar molecules are used for low energy bandwidths, strong and wide absorption. Power efficiency of solution-processed OSCs based on N (Ph-2T-DCNMe) 3: PC 70 BM (1: 2, wt%), 4.76% and filling factor 56%, under AM1.5G, 100 mA −2 cm was obtained. N (Ph-2T-DCNMe) 3, which has the methyl terminal group, exhibits wider absorption in better membrane shape and greater mobility by incorporating PC 70 BM, longer carrier life and charge. [23]

While researching polymer solar cells, Serkan Ensiner and his colleagues designed a poly (dimethylsiloxane) (PDMS) tissue almost prismatically designed to extend the optical path of light into the absorbent layer and reflection inside the cell with this structure. . PDPPTPI was used as electron donor and PCBM as electron acceptor. Also ITO with poly (3,4-ethylenedioxythio

phene): poly (styrene sulfonate) (PEDOT: PSS) was coated. Comparison of the results obtained with the use and non-use of the polymer plate showed that the conversion efficiency of this cell increased by 19%. Optical simulation was performed by Mathematical expression of transfer matrix by Setfos software. [25]

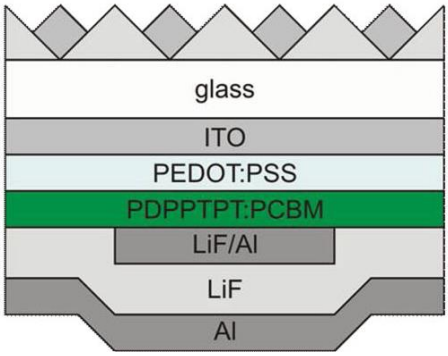

Figure 4.4- Organic solar cell powered by Ensiner, which increased polymeric tissue anchorage efficiency by up to 19% by placing polymeric tissue on top of the cell.

One of the simulation work carried out by Boland et al. Was to study the numerical study on tandem cells by examining two components of P3HT: PCBM and PCPDTBT: PCBM. They looked at the electrical properties of the cell in tandem with an efficiency of about 9%. The reason for their use of these two composites is because of the difference in absorption between the two materials, which makes the cell work in a wider range of light. {} Also, Koster et al. Its efficiency was estimated at 2.5%. To achieve this, they only modeled and simulated the active layer.

Conclusion

Based on the results obtained in the present study, three types of OC1C10PPV: PCBM and P3HT: PCBM and PCPDTBT: PCBM materials were synthesized, simulated to evaluate their performance and cell efficiency. Finally, the simulation results are compared with the results in the literature.

Chapter Three
Organic solar cells

Types of solar cells

Solar cells can be divided into two distinct categories: conventional solar cells, such as silicon p-n junction and excitonic solar cells or XSC (Excitonic Solar Cells). Most organic-based solar cells, including DSSC (Dye-Sensitized Solar Cells) and Polymer-Inorganic Hybrid Cells, fall into the category of XSCs. In these cells, electron excitation by light absorption produces a bound electron-hole pair, called exciton. Although excitons are not directly produced in heterogeneous substrates, they must be scattered in this substrate to produce photogeneration of charge carriers. This is a distinctive feature of XSCs, which are load carriers immediately after production, separated into a dual common season. In conventional cells, in contrast, the photon generation of the free electron-cavity pair occurs in bulk semiconductors, and charge separation, which is based on their entry into the junction, is a subsequent process. This seemingly small distinction results in substantial differences in photovoltaic behavior [3].

3.2 Examples of Organic Materials-Based Solar Cells

A variety of organic material-based solar cells include:

- Color-Sensitive Solar Cells
- Polymer solar cells

Solar cells are based on Liquid Crystals.

How Organic Solar Cells Work

The absorption of sunlight in organic molecular semiconductors results in the formation of molecular excitons and is excited by a bipolar and singular ground state process into a single molecularly excited exciton. This exciton is confined to a single molecule, which is generally at the nanometer scale. The current flows if the exciton can be disrupted and the hole and electrons are ejected. In contrast, photon absorption in organic semiconductors used in solar cells results in separate cavities and electrons that flow freely and independently of each other, and thus play a direct role in the current flow.

One of the main problems in the development of organic solar cells is overcoming localization and coupling in the form of excitons of electrons and holes produced by light. Once the exciton is disrupted, it can often flow from molecule to molecule, a hopping process. Materials and structures designed to facilitate exciton disruption are key to the success of organic solar cells.

The simplest organic solar cell structure is a single-layer fragment (Fig. 7). Photons create molecular excitons in the organic semiconductor layer. This piece relies on different work functions between the cathode and the anode to create a large electric field to collect these charges.

The carrier diffusion length is generally about 10 nm and the thickness of the semiconductor layer is much greater than 10 nm to obtain acceptable photon absorption. The majority of excitons produced are never discrete and only a small fraction of the carrier produced is collected by the electrodes. In fact, the electric field is only high at the sudden joint surfaces of the conductor - semiconductor, and here the exciton breakdown can occur with ease. However, efficient carrier collection requires the presence of both types of carrier. [18]

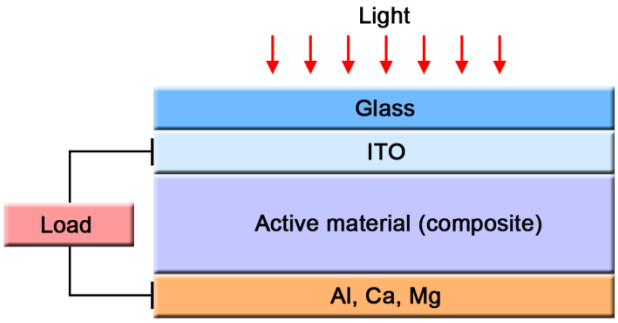

Figure 3-1- Single layer organic solar cell

Significant increases in charge collection can be achieved using flat solar cells with heterogeneous junction (BHJ). The addition of an electron transfer acceptor layer (ETL) and a hole transfer transducer (HTL) give rise to a strong electric field at the interface of the heterogeneous junction, which greatly facilitates the exciton disruption there. In principle, both the donor and acceptor layers can Attract photons and fill with exciton. These excitons can then be propagated to the common surface of the heterogeneous bond and disrupted there.

The sharp and narrow field region at the interface of heterogeneous junction in organic solar cells can be compared with the inorganic p-n junction. The width of the empty region (energy gap) in the inorganic junction is determined by the spatial distance at which the carriers are recombined to maintain equilibrium. At the organic organic level in organic bonds, the charge carriers in the LUMO and HOMO levels are transported from one molecule to the other by mutation and only minimal charge transfer occurs, leaving the equivalent of the empty region with very little thickness. The potential difference between the HOMO and LUMO levels lies in a very small spatial dimension in nanometers and generates a strong electric field in the junction.

However, the donor layer is actually designed to absorb photons and fill the exciton. Because the mobility of the cavities is relatively higher than the electrons, the HTL donor allows the cavities to diffuse to the surface of the heterogeneous bond. Electrons are bound to holes, because the exciton breaks down as long as the excitons do not reach the common surface. This common surface now allows the collecting of electrons and holes, the electrons and holes being driven to the holes layers, the holes reaching the ITO electrode through the conductive layer of the hole, and the electrons The electrodes reach the cathode through the conductive layer of the electron.

The donor and acceptor terms used to describe the heterogeneous bond constituent two layers are proposed because the electrons that are disrupted in the donor bond in the bond are transferred or

transduced from the donor molecule into the bond molecule. Are accepted by the acceptor molecules in the acceptor layer. Discrete cavities of excitons remain in the donor layer and are driven to the anode. These terms are similar to the molecular donor and acceptor terms used in impurities used in inorganic semiconductors: however, organic molecules give and receive electrons to neighboring molecules, not electrons and energy bands. They. Since the acceptor layer is full of electrons, this layer must be conductive to the electron and carry the charge at its LUMO level. Conversely, the donor layer, which is of the cavity, must be the conductor of the cavity and these holes are carried in its HOMO level.

The thickness of the p-type layer is controlled by the propagation length of the excitons that must reach the interface in order to be discrete. The donor layer, which is very thick, lowers yields because a significant fraction of the excitons produced are re-combined before reaching the common surface. A layer that is too thin results in less light absorption. Using a flat heterogeneous junction design, only a few percent of solar cell efficiency can be achieved.

Since the diffusion lengths in organic matter are approximately 10 nm, the useful absorption depth in the donor layer is only 10 nm, which means incomplete absorption of sunlight limits the performance of the solar cell with heterogeneous junction. The thickness required for almost complete absorption of sunlight in organic matter is about 100 nm, however, a donor layer of this thickness has poor efficiency, and most excitons produced are reconstituted without reaching the common surface. Due to the high energy band gap in organic matter, only a small fraction of the sunlight is absorbed. The exciton penetration length should be as large as the phase separator-receiver separation. Otherwise, the excitons disintegrate through the irradiated or non-irradiated pathways before they reach the common surface. The penetration length of excitons in organic semiconductors and polymers is usually about 10 to 20 nm. Mixing conjugated polymers with electron acceptors such as fullerenes is a very effective method of fitting excitation light excitons to free charge carriers. Studies of physical light have shown that the transfer of excitation light in such mixtures will be much faster than competing relaxation processes [13].

A successful way to further improve performance is to arrange several joint surfaces in the light path and thin each donor layer to allow the effective exciton diffusion to the nearest heterogeneous joint interface. Part of the sunlight is absorbed into each thin layer of light and the remaining light can reach the next layer. This method relies on a layer of heterogeneous volumetric bond (BHJ), a layer comprising several donor and acceptor regions. (Figure 8)

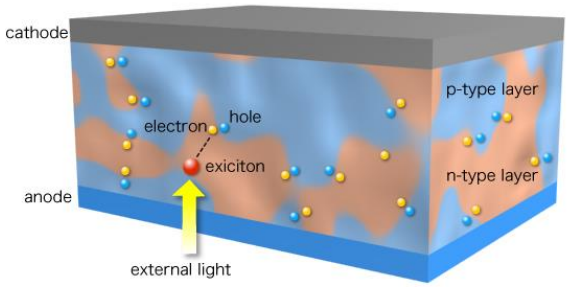

Figure 3.2 Solar cell with heterogeneous organic volumetric bond

The volumetric heterogeneous bonding layer can be formed using a variety of nanostructures, and the invention of techniques and materials to achieve these nanostructures has been at the heart of the effort to further improve organic solar cells. Solar cells with heterogeneous volumetric bonding have achieved the highest efficiency in organic solar cells using a single organic absorption band for light absorption.

The optimum nanostructures length scale is about nanometers, and the use of self-organizing organic materials to achieve a low-cost way of creating these nanostructures is considered. For example, donor and acceptor organic matter can be mixed and then deposited on the substrate of the solar cell. If the blend material is spontaneously dissociated under appropriate conditions to form a heterogeneous volume junction, then self-organization is achieved. This reduces the cost of processing significantly, as no micromicroscope modeling and lithography techniques are used. Although these inorganic semiconductor component processing techniques are well known and highly developed, they are not cost effective for large-scale solar cells.

One of the important prerequisites for heterogeneous volumetric bonding is the substrate for conduction of the effective output current from the donor and acceptor regions and the collection of this current by the electrodes. Two specific examples of heterogeneous structures are shown below. Figure (a) shows a morphology that limits the efficiency of current collection because the donor and acceptor layers are not well attached to the electrodes. Figure (b) shows a more favorable structure because the donor and acceptor materials are arranged to allow effective bonding to the electrodes.

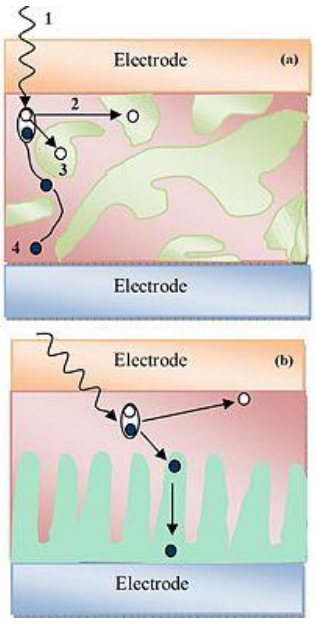

Figure 3.3- Volumetric heterogeneous junction, acceptor and random donor zones b) Volumetric heterogeneous junction, acceptor and donor zones

Another important area of flow development relates to the use of organic multilayer solar cells, in which different layers act in a similar way to inorganic multinucleated solar cells to absorb different parts of the solar spectrum. This is particularly important for organic solar cells, because the bandwidth of the absorption band for a given organic matter is small. This is because the π and π * bands are much narrower than the conductivity bands and the capacitance in inorganic semiconductors. And this limits the absorption bandwidth.

The heterogeneous bond structures discussed, if excitons can be produced and collected in the donor and acceptor materials, can provide two absorption bands. The energy gaps of these two layers can be different, and the form of this approach involves achieving large transmission lengths in the donor and acceptor layers and efficient carrier collection. An organic material that has all the features necessary for an ideal acceptor - including good electron mobility, high optical absorption, and effective electron capture from the donor - has yet to be found.

To date, efficiencies of about 7% to 8% have been achieved in the laboratory environment for organic solar cells.

Materials used

Organic compounds

Organic compounds are any kind of material and chemical composition (solid-liquid-gas) that contain carbon in their molecules. This is not a general definition and does not include all carbon compounds such as carbide, elma, cyanide and simple carbon oxides. The compounds mentioned above, although carbon-bound, are in the category of mineral composition. Today, most materials are composed of two elements, carbon and hydrogen, organic matter.

Cathode materials

Unlike anodic, cathode materials are generally not transparent, and this leaves us open to a variety of materials. These materials should be of high conductivity and low in function and adhere well to the underlying polymeric layers. Stability is also important and largely depends on the framing.

Challenges to cathodes include easy oxidation resulting from the use of low-performance materials that require Group 1 and Group 2 metals that are easily ionized. These cathode layers also tend to undergo chemical resuscitation of adjacent organic layers. Like polymer OLEDs, the double-layer cathode is also used here, and is widely used in the LiF / Al structure in which aluminum protects the reactive LiF layer and provides improved plate conductivity. The formation of LiF maintains the low cathode work function but reduces the tendency to mix with oxygen as a result of the reaction with the organic EIL. The working function of LiF / Al cathodes is between 3.6 and 3.8 eV. The cathode layer is usually the most reactive layer in the cell when oxygen or water is present.

Anodic materials

The ITO anode provides easy patterning and good stability. The smoothness and smoothness of the ITO substrate and layer, as well as those in the polymer OLEDs, are important. Surface roughness and roughness of less than 2nm are generally required. The ITO has a high working function (□> 4.1eV) that enables it to inject holes efficiently. The ITO's transparency is as a result of its wide bandwidth of more than 4eV.

There are challenges and challenges to using ITO for micromolecular cells and OLEDs. The ITO has a resistivity of □2 * 10-1□ that limits the flow of current inside the ITO layer and leads to unwanted voltage drop during anodic conductors. ITO is necessarily rough and rough due to its multi-crystals. ITO has a chemically active surface that indium shifts to the next polymeric layers. The ITO task function is sensitive to the cleanup process used to prepare ITO for subsequent processes. ITO is a thin, brittle, inorganic layer that is not ideal for polymer substrates, since ITO usually requires high temperatures for the substrate (200-4000C) and may crack on polymers due to thermal and mechanical deformation. . However, ITO is still the most common anodic material for organic solar cells.

3-5 Common Polymers Used

3-5-1-Donor

Many conjugated polymers have been tested as active ingredients for solar cells. But the most common organic conjugated polymers are poly (3-hexyl thiophene), (P3HT) poly (2-methoxy-2-(2-ethylhexyl oxy) -1 and 4-phenylene vinylene), (MEH-PPV). (Poly (2-methoxy-1- (3- and 7-dimethylactyl oxy) -1) and 4-phenylene vinylene (MDMO-PPV) having a conjugated polyphenylene vinylene (PPV) core (Fig. 10). PPV alone is an insoluble material. And the increase of alkyl or alkoxy groups on the phenylene ring in MDMO-PPV and MEH-PPV makes these materials processable and soluble in some organic solvents such as chloroform, chlorobenzene or 2 and 2-dichlorobenzene [3].

A common thiophene-based donor is P3HT. It is soluble in several organic solvents, making it suitable for low-cost solution processing. The other donor material is PQT-12 (poly (3 and 3 "-diododecyl quaterti ...

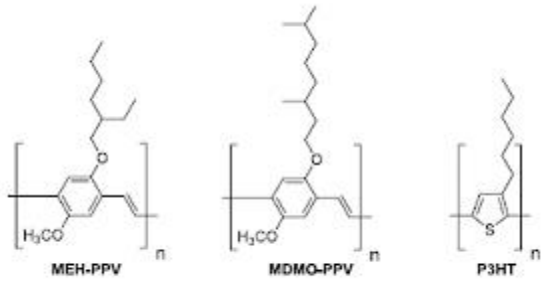

Figure 4.3- Common conjugated polymers used in organic solar cells

Other polythiophene materials that are widely used in organic solar cells include PEDOT: PSS or poly (2 and 2-ethylene oxy thiophene) (polystyrene sulfonate). A thin layer of PEDOT: PSS is commonly used as the cavity conductor material directly above the electrode (Indium Tin Oxide, ITO) [3]. Examples of polythiophenes used in solar cells are shown below.

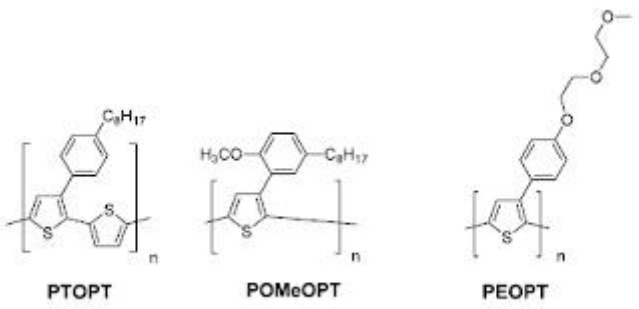

Figure 3-5 Polythiophene materials used in organic solar cells

3-5-2- ACCEPTOR

Acceptors or acceptors can be small molecules or polymers. Electron affinities are high electron affinity and have good electrical conductivity but do not require light absorption, including C60, or a molecule composed entirely of carbon, and soluble derivatives. Fullerenes are the most widely used receptors due to their high electron demand and efficient charge transfer capability and are in fact the best electron acceptors to date. Graphite surfaces, such as C60, allow efficient local unbound electrons to be transported to molecular orbitals leading to LUMO alignment.

Fully soluble derivatives are used for this purpose, and PCBM is a highly soluble methanofluorene derivative ((1 and 2) - (phenyl-C61-butyric acid methyl ester). Results in tool performance.

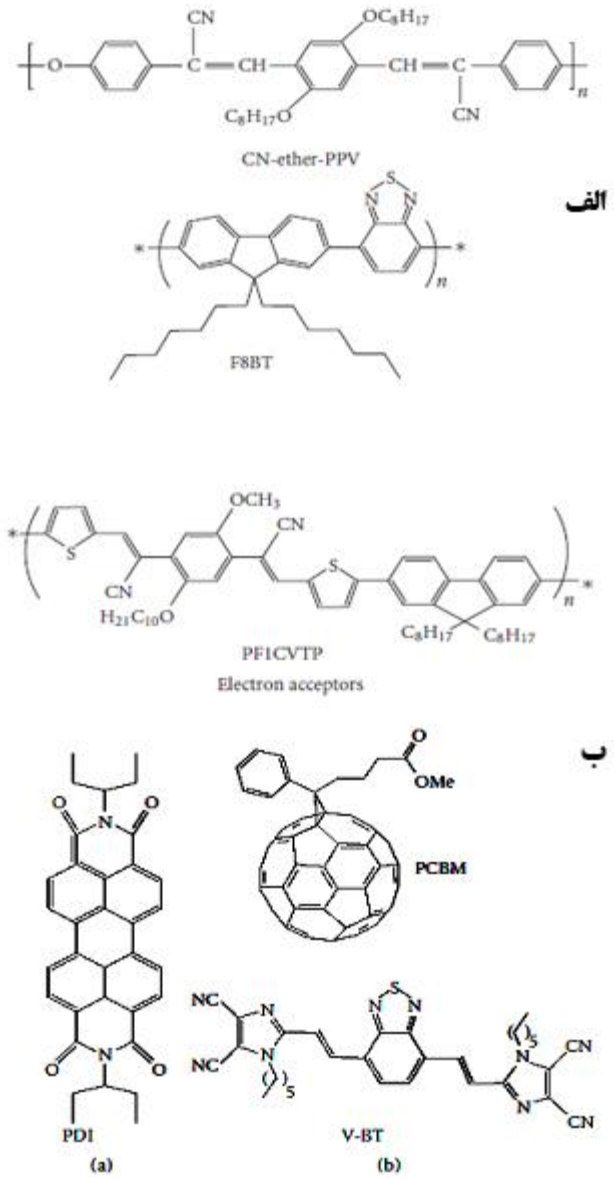

Figure 3.6- A number of common receptors a) polymeric receptor b) small molecular receptor (7)

C60s are excellent acceptors because they have LUMO levels of electron energy well below the vacuum level, and especially below the LUMO levels of various donor molecules required for solar cells. This property is required for an acceptor molecule. In fact, each C60 can accept multiple electrons through the gaps in the LUMO balance. Electron transfer in a C60 molecule is very fast and efficient. The electrons inside the molecules are quasi-stable and therefore easily transferred to the solar cell electrode. Finally, C60s have a absorption spectrum that reaches its peak in the ultraviolet portion of the spectrum, which means that they provide only minimal absorption in important portions of the solar spectrum and provide the donor layer to absorb visible or infrared solar radiation. they let.

Carbon nanotube is another acceptor of interest. One promising development is the use of carbon nanotubes as acceptors. The nanotubes, consisting of tubular graphite plates, have electronic properties similar to those of C60.

Electrical Characteristics of Organic Solar Cells

The most important electrical properties to measure a cell include:

• Voc Open Circuit Voltage: Voltage below zero current density

• Jsc Short Circuit Current: The current density of a cell at zero applied voltage

• FF Performance Factor: FF = (Jmax xVmax) / (Jsc x Voc)

• Power conversion efficiency (η): η = Pout / Pin = (Pmax / Plight) x FF = (JscxVoc) / Plight

Methods for improving the efficiency of polymer solar cells

What is important about polymer solar cells is improved efficiency, light absorption, and the production of new structures with varying morphologies, increased flexibility and environmental stability. Today, the focus of scientists is on increasing the efficiency of polymer solar cells. Among the most important factors that can be used here are the type of polymer used to improve the efficiency of polymer solar cells:

• Improved absorption

• Improved Voc

• Structure control

• Using quantum dots

Over the past two decades, a number of organic materials used in organic solar cells have been designed, combined and used. Therefore, the development and improvement of active layer materials is the key to improving efficiency. In order to obtain better photovoltaic properties, some properties such as energy band gap, molecular energy level, mobility, solubility, etc. are especially considered in active layer materials and how these parameters are balanced is one of the most important parts for molecular design. Is.

Disadvantages and Benefits and Applications of Polymer Solar Cells

Among the benefits of polymer solar cells over other types of solar cells can be the low cost of production, the large surface area, the flexibility, as well as the disadvantages of this generation, the low electron flow, absorption characteristics that are not suitable for the sun's spectrum. , Environmental degradation, etc., point to the importance of achieving low-cost solar cells Researchers are working to improve the efficiency of this generation and eliminate its disadvantages. Solar cells made of organic matter have much lower yields than their silicon counterparts. But because of the low cost of construction, as well as capabilities such as flexibility, they are suitable for non-industrial applications. Portable mobile chargers, battery packs on curved surfaces such as car bodies, and even their use in clothing, are foreseen for organic solar cells.

Their other feature is the flexibility along the wave with the highest absorption. As a result, if organic matter is absorbed by infrared, organic solar cells can be used in car glass, home glass and any other place that should be transparent.

Conradka, Plex Tronic, Hliatek are working to industrialize these solar cells.

The lifetime of organic solar cells, especially for samples without protective layers, is very low. For example, the lifespan of cells in which they use BCP as an excitation barrier layer is approximately several hours. Although the reasons for the short life span in organic cells have not yet been fully elucidated, it can be attributed to the following factors:

1. Destruction of organic matter (especially polymers) by exposure to high temperatures or when exposed to light.

2- Reduction of fullerene conductance (C60) (used as an acceptor in almost all types of organic cells) by oxygen uptake

3. Chemical changes of the electrodes

4- Physical changes (eg morphology) of organic matter

Therefore, it seems that the existence of protective layers against air and moisture is essential for long-lived cells. The lifetime of the first commercial organic solar cells produced by Konaraka is 2 years, the longest reported lifetime for organic cells.

Chapter Four
Organic solar cell simulation

Introduction

In this study, we investigated the simulation of organic solar cells. To simulate the COMSOL environment, we first consider an experimental sample and simulate the results obtained with the experimental results. In this study, formulas, carrier concentrations, electrical potential, and finally organic cell efficiency were investigated, followed by a brief review of the role of contact information, drift, charge carrier penetration, charge carrier and re-hybridization. In another part of this study, by modifying the active layer material, we examined the results mentioned in the previous section with the results obtained from the new material. All these steps were performed with the help of COMSOL Multiphysics software. To define the electrical model of these BHJ solar cells using COMSOL software, with the help of Poisson's equation and electron and hole continuity equations, a voltage-current diagram was obtained and then the power diagram and finally FF and cell efficiency were obtained. In addition, changes in wavelength quantum efficiency as well as short-circuit current changes due to thickness changes of the active layer are discussed.

4.2.2 Solar cell simulation study

First, a brief description of the model is given, followed by an overview of the relevant equations, and then the mechanism of generating the free load carriers that complete the model description.

In the experimental method, the organic solar cell under investigation is composed of glass, ITO, PEDOT: PSS, active layer and finally aluminum / lithium fluoride. Active layer of poly [2-methoxy-5- (3 ', 7'-dimethyloctyloxy) -p-phenylene vinylene] - (OC1C10-PPV) and [6,6] -phenyl C61-butyric acid methyl ester- (PCBM) With a ratio of [1: 4 wt. %] Created as a BHJ solar cell / polymer cell, calculations were performed at room temperature and in nitrogen atmosphere. A white halogen lamp of about 800 W / m2 was used to irradiate the device. The results obtained from the simulation are discussed with the results obtained from the experimental results (carrier density graphs and electric potential and efficiency value). In the next section of the material investigated in the active layer of poly [2,6- (4,4-bis- (2-ethylhexyl) -4H-cyclo-penta [2,1-b; 3,4-b0] dithiophene) - alt-4,7- (2,1,3-benzothiadiazole)] (PCPDTBT) and (PCBM-) poly (3-hexylthiophene) (P3HT)) and (PCBM), a polymer with a small band gap, with a ratio of [1: 4 wt. %] And] [1: 1 wt. The% was tested and its results compared with the first simulated cell to finally select the ideal solar cell from among them in terms of efficiency. It should be noted that the amount of P3HT: PCBM efficiencies obtained in the experimental results are compared with those obtained in the simulation. Finally, according to the model obtained from the prototype, we simulate PCPDTBT: PCBM in COMSOL software environment.

Table 4-1 - Thickness of organic solar cell components studied

Components	Thickness
Glass	
ITO	140nm
PEDOT: PSS	25nm
OC_1C_{10}-PPV: PCBM Or PCPDTBT: PCBM	120nm
P3HT: PCBM	100nm
Aluminum / Lithium fluoride	100nm

In the experimental study performed for the production of active layer, (OC1C10-PPV) and PCBM were used as test specimens with the new method. First, the PCBM polymeric composition was transferred as a spin coating from a chlorobenzene solution onto the substrate. Sample (OC1C10-PPV): PCBM was exposed to vacuum for 1 h at room temperature to remove excess solvent. Thickness measurements were performed using a Dektak surface profiler calibrated from a SiO2 ellipsometry standard.

The aluminum electrode at the top of the device acts as a cathode and collector of electrons. Titanium oxide acts as an electron transducer, cavity barrier and optical separator that changes the amplitude of the optical field inside the active layer. (PEDOT: PSS) Cavity Transducer and Indium Thin Oxide (ITO) acts as the cavity collecting anode.

To simulate the solar cell with active layer (OC1C10-PPV): PCBM in COMSOL environment and investigate the current-voltage and cell efficiency characteristics, we used one-dimensional modeling to define the electrical properties of this active material. (Definition of the electrical properties of the active layer in one dimension is less reliable than the two-dimensional and three-dimensional modes.) This simulation was performed at wavelengths between 300 and 800 nm under 1.5 G AM conditions. .

For this simulation, the thickness of both active layers, (OC1C10-PPV): PCBM and (PCPDTBT): PCBM, was assumed to be 120 nm but for P3HT: PCBM 100 nm. Temperature was assumed to be 298 K and 9.9931 * 1014 1 / s. The following table summarizes the other parameters that are assumed to perform this constant simulation.

Table 4-2- Fixed parameters used in all three composites

Parameter	Formula	Definition
phi_anode	1 [this]	Anode Working Function
phi_cathode	2.34[this]	Cathode work function
energy_binding	[eV] 0.28484	Energy connection
T.	298 [K]	Temperature
lambda	[nm] 300	Wavelength
freq	c_const / lambda	Frequency
V_app	[V.] 0	Applied voltage
Area	[m ^ 2] 1	Area
affinity	1 [V]	You want an electron
switch	2	

It should be borne in mind that by changing each of the fixed parameters used for all three composites, especially the amount of electron demand that can be varied in efficiency and other outputs by varying the values for different materials as one of the baser properties and indexes. Desired results.

Electron acceptor and electron acceptor energy scheme in composite (OC1C10-PPV): PCBM is given in the following figures:

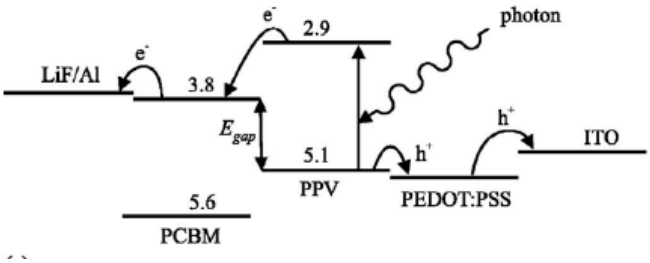

Figure 4-1- a) Scheme of electron donor materials and acceptors (energies given in volts). After the charge separation, electrons and cavities are transferred through the respective materials and collected by the electrodes. The anode of a poly (3,4-ethylenedioxythiophene) / poly (styrenesulfonate) (PEDOT / PSS) layer on the ITO (Indium Thin Oxide) precipitate was used, while at the top of the active layer, the Lithium fluoride and aluminum are precipitated by vacuum thermal evaporation.

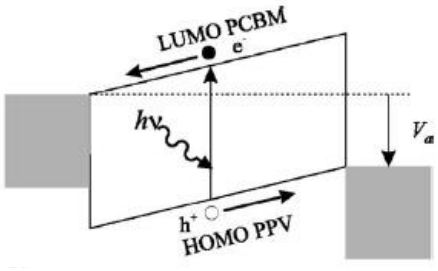

Figure 4-2- (b) Model of the device obtained in a metal / insulator / metal representation with positive bias applied under Va under operating conditions (Va is smaller than open circuit voltage).

4.3- Governing Equations

The basic equations used in this simulation are Poisson's equations, Equation 2:

$$\frac{\partial^2}{\partial x^2}\boldsymbol{\psi}(\boldsymbol{x}) = \frac{q}{\varepsilon}[\boldsymbol{n}(\boldsymbol{x}) - \boldsymbol{p}(\boldsymbol{x})]$$

Where q is the fundamental charge and ε the dielectric constant dependent on the potential ψ (x) of the electron and hole densities n (x) and p (x), respectively. Flow continuity equation, Equation 3:

$$\frac{\partial}{\partial x}J_n(x) = qU(x)$$

$$\frac{\partial}{\partial x}J_p(x) = -qU(x)$$

Where Jn (p) (x) is the electron current density (cavity) and U (x) the net rate of production, ie the difference between the production and recombination of free carriers. In the rest of this research, the X dependencies of variables are omitted for written convenience, unless noted. Only one spatial dimension is considered, as the device has a very small flat structure (typically 100nm) compared to lateral dimensions (typically several millimeters).

To solve the basic equations, a set of current density dependent equations is required for carrier densities and potentials. The combination of both thrust and infiltration of load carriers is one, Equation 4:

$$J_n = -qn\mu_n\frac{\partial}{\partial x}\psi + qD_n\frac{\partial}{\partial x}n$$

$$J_p = -qp\mu_p\frac{\partial}{\partial x}\psi - qD_p\frac{\partial}{\partial x}p$$

Where Dn, p are the carrier propagation coefficients assumed to follow Einstein's equation, Equation 5:

$$D_{n,p} = \mu_{n,p} V_t$$

Where Vt is the thermal voltage, ie Vt = kBT / q where kB is the Boltzmann constant and T is the absolute temperature. Note that at high carrier densities, the diffusion coefficient may increase.

To obtain a unique solution to the system of equations consisting of Equations 2-5, it is necessary to specify the carrier densities and potentials in both equations. The call at x = 0, where x represents the position inside the device, is called the top contact, and the call at x = L, where L is the end contact of the device. It is assumed that the top contact with the conductor strip from the semiconductor to the line is therefore ohmic. Using Boltzmann statistics, equation 6:

$$n(0) = N_c$$

$$p(0) = N_c \exp(-\frac{E_{gap}}{V_t})$$

Where Nc is the effective state density in both conduction and conduction bands. This indicates that the contacts are in thermodynamic equilibrium, compared to the rest of the device. Since the exact values of effective density of states for conduction band and capacitance are unclear and of little importance, a value has been used for both bands. Similarly, the terminal contact is assumed to be the ohmic cavity. Therefore, Equation 7:

$$n(L) = N_c \exp(-\frac{E_{gap}}{V_t})$$

$$p(L) = N_c$$

The ohmic nature of both contacts is proved by the measurement of the voltage current, which clearly shows the limited charge-space behavior. The boundary conditions for the potential are as follows, Equation 8:

$$\psi(L) - \psi(0) = E_{gap} - V_a$$

Where Va is applied voltage.

Production and recombination

Photogeneration of free carriers is defined by the combined recombination of the onsager theory. By refining this theory, Braun proposed a new definition by referring to the bound electron-hole pair, which acts as a novel material for free charge carriers, with a limited lifetime. Figure 15:

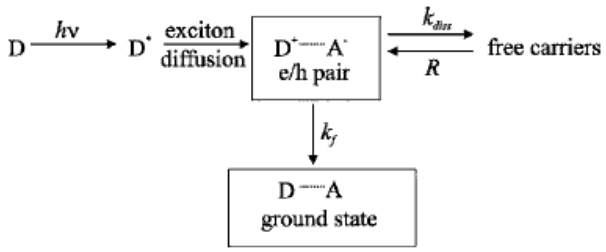

Figure 4-3. Schematic of charge carrier separation in the joint layer of the donor and receiver layers. After the stimulant, exciton is created which is released by the mediator until it reaches the common season. In the common season, the electron is transferred to the receiver thereby forming a bound electron-hole pair. The pair can also be separated into free carriers or decayed into ground state.

The bound electron-hole pair may degrade to the ground state with the rate of Kf decay or separation into free carriers. Separation to free carriers is actually a competition between separation (kdiss constant rate) and recombinant (constant R rate) which restores the charge transfer mode. In the Brownian model, the probability of electron-hole pair separation for the given electron-hole pair is x, as follows, equation 9:

$$p(x,T,F) = \frac{k_{diss}(x,T,F)}{k_{diss}(x,T,F) + k_f(T)}$$

Which depends on the temperature T and the intensity of the electric field F. Based on the Onsager's theory of constant-field-rate dissociation rate for weak electrolytes, Brown deduces the following expression for kdiss, equation 10:

$$k_{diss}(x,T,F) = \frac{3\gamma}{4\pi a^3} e^{-E_B/k_B T} J_1(2\sqrt{-2b})/\sqrt{-2b} = \frac{3\gamma}{4\pi a^3} e^{-E_B/k_B T}(1 + b + \frac{b^2}{3} + \cdots)$$

$$b = q^3 F/(8\pi\varepsilon k_B^2 T^2)$$

That EB is the coupling energy of the electron-hole pair, J1 is a type 1 Bessel function. The bimolcular recombination rate R is used, equation 11:

$$R = \gamma(np - n_{int}^2)$$

Where $n_{int} = N_c \exp(-\frac{E_{gap}}{2V_t})$ is the intrinsic density of the carrier electron and the cavity. The recombination intensity is obtained by Langevin, Equation 12:

$$\gamma = \frac{q}{<\varepsilon>} <\mu>$$

Where <μ> the spatial average of the sum of electron and hole motions is the dielectric constant of the constant ε. The decay rate of the electron-cohesive coupling at the ground state, kf, is a suitable parameter. As polymer systems subject to disturbance, it is reasonable to assume that the electron – hole coupling distance within the system is not constant. As a result of Equation 9, there must be more than one integrated separation distance distribution, Equation 13:

$$P(a,T,F) = \int_0^\infty p(x,T,F) f(a,x) dx$$

Where f (a, x) is a function of the normal distribution as follows, equation 14:

$$f(a,x) = \frac{4}{\sqrt{\pi} a^3} x^2 e^{-x^2/a^2}$$

In the rest of the research, the dependencies of a, T, F of P for written convenience have been reduced.

It should be noted that the Onsager-Brown theory is applicable to the calculation of exciton separation while describing the molecular hybrid in the open langon relation. Both results are combined as one-dimensional and augmented propagation and thrust models by the exciton continuum equation so that the flow efficiency and current density can be determined ().

Suppose that G is bound to the rate of electron-hole pair production. Then the number of X-electron-cohesive pairs per unit volume varies with time, Equation 15:

$$\frac{dX}{dt} = G - k_f X - k_{diss} X + R$$

A similar equation was used by Barker and his colleagues, when they consider the separation of charge-carrier pairs in a bilayer photovoltaic device, in the steady state this equation will be equal to, Equation 16:

$$G - k_f X = k_{diss} X - R$$

That is the density of the net number of free carriers produced. Consequently, the equation of continuity for the electron will be Equation 17:

$$\frac{dn}{dt} = \frac{1}{q} \frac{\partial}{\partial x} J_n + k_{diss} X - R$$

Using the relation 9, kdiss = [P / (1 − P)] kf, so the relation becomes 16, equation 18:

$$k_{diss}X = PG + PR$$

And finally the equation of continuity, Equation 19:

$$\frac{1}{q}\frac{\partial}{\partial x}J_n = PG - (1 - P)R$$

This means that after the two-molecular recombination, the carriers do not necessarily lose, but the first form of a bound electron-cavity pair that can either be re-incorporated into free carriers or decay into bases, in this case carriers They will not disappear. Finally the rate of net production is given by Equation 20:

$$U = PG - (1 - P)\gamma(np - n_{int}^2)$$

Introducing COMSOL software

COMSOL is a powerful environment in which to model various scientific and engineering problems and, based on Partial Differential Equations (PDE) models to describe models of various problems with their corresponding physical quantities such as Examined the parameters and properties of the materials and more. These related variables and numbers can be directly entered into the area of objects, boundaries, edges, and nodes that are independent of the mesh being computed. COMSOL then starts assembling a set of PDEs defined by the model itself. Graphical User Interface This software is one of the strengths that provides a graphical environment for user interaction for modeling in this software. In fact, the software communicates with the user-designed model by the graphical environment and then analyzes the model based on physical modes, PDE modes, or a combination of the two. Various analyzes can be performed using the physics interfaces provided to the user. Among these analyzes are the following:

• Static analysis and time function

• Linear and nonlinear analyzes

• Frequency, modal and frequency response analysis.

PDEs are in fact the basis of scientific laws and many of the scientific and engineering phenomena are modeled on them. The basis for the operation of real physical phenomena is the simultaneous coupling of multiphysical PDEs to a system. For further explanation, this example is noteworthy: In nature, the transmission of electric currents is often accompanied by an increase in ambient temperature. To illustrate the effect of current flow on how heat is transmitted and distributed in the environment, the two physical phenomena of electric current and heat distribution must be analyzed simultaneously. For this reason, COMSOL can be widely used in various scientific fields.

The scope of this software includes sciences such as: acoustics, electromagnetism, fluid dynamics, heat transfer, optics, photonics, semiconductors and more.

Many of the multiphysics interfaces already defined in this software make it easy to use, especially in multi-physical applications. The power of modeling and analysis is a key feature of COMSOL in a wide range of applications.

4-6- How to do it

To simulate bulk heterojunction solar cells in COMSOL environment, we tested the simulation of organic matter in the active layer. To begin with, the semiconductor module is used because the semiconductor interconnection chapter uses Poisson's equation to solve the drift and diffusion potentials for electrons and holes in a semiconductor material. , Used. Small signal-frequency domain analysis was used to study the semiconductor module in COMSOL environment. This analysis is used to study small fluctuations in a bias-based solution in electromagnetism. This study consists of two basic steps: 1) a static and stationary study, followed by a frequency domain to solve the bias, and 2) a disorder study, to calculate the response to the bias. It also calculates the disorder, with a linear disorder to solve the bias. Here, our model is examined nonlinearly.

The following requires a detailed definition of the organic material parameters used in the active layer and other parameters affecting this cell, listed in Tables 4-5-4. The tables show the properties of three different groups of these composites. It should be borne in mind that each material has its own unique properties. Although some of these parameters and properties change with its structural (molecular-level) engineering such as the energy bandwidth, these changes are still stable to the material itself and improve the efficiency of that material in the devices and structures used.

Table 4-3- Input Parameters and Formulas for OC1C10PPV Composite: PCBM

Parameter	**Formula**	**Definition**
L.	[nm] 120	Thickness
E_gap_PPVPCBM	[V.] 1.34	Energy gap
mun_PPVPCBM	2.5e-7 [m ^ 2 / (V * s)]	Electron mobility
mup_PPVPCBM	3e-8 [m ^ 2 / (V * s)]	Cavity mobility
N_c_PPVPCBM	2.5e25 [1 / m ^ 3]	Navigation bar
epsilonr_PPVPCBM	3e-11 [F / m] / epsilon0_const	forgiveness Relative
a_PPVPCBM	[nm] 1.3	The average distance traveled by the mean electron and hole
kf_PPVPCBM	1.5e6 [1 / s]	object Vapa rate
gamma_PPVPCBM	e_const / (epsilonr_PPVPCBM *) epsilon0_const)) * (mun_PPVPCBM + (mup_PPVPCBM	Effective mobility of electrons and cavities
n_init_PPVPCBM	sqrt (N_c_PPVPCBM ^ 2) * exp (-e_const * E_gap_PPVTPCBM / (2 * k_B_const * T))	Thermodynamic equilibrium concentration

Table 4-4 Input Parameters and Formulas for PCPDTBT Composite: PCBM

Parameter	Formula	Definition
mun_PCPDTBTPCBM	3e-3 [cm ^ 2 / (V * s)]	Electron mobility
mup_PCPDTBTPCBM	4.5e-4 [cm ^ 2 / (V * s)]	Cavity mobility
E_gap_PCPDTBTPCBM	[V.] 1.24	Energy gap
epsilonr_PCPDTBTPCBM	3.4	forgiveness Relative
N_c_PCPDTBTPCBM	2.5e19 [cm ^ -3]	Navigation bar
a_PCPDTBTPCBM	[nm] 1.47	The average distance traveled by the mean electron and hole
kf_PCPDTBTPCBM	1e5 [1 / s]	object Vapa rate
gamma_PCPDTBTPCBM	e_const / (epsilonr_PCPDTBTPCBM *) epsilon0_const)) * (mun_PCPDTBTPCBM + (mup_PCPDTBTPCBM	Effective mobility of electrons and cavities
n_init_PCPDTBTPCBM	sqrt (N_c_PCPDTBTPCBM ^ 2) * exp (-e_const * E_gap_PCPDTBTPCBM / (2 * k_B_const * T))	Thermodynamic equilibrium concentration
L.	[nm] 120	Thickness

Table 4-5- Input parameters and formulas for P3HT: PCBM composite

Parameter	Formula	Definition
L.	100 [nm]	Thickness
E_gap_P3HTPCBM	1.9 [V]	Energy gap
mun_P3HTPCBM	1e-5 [m ^ 2 / (V * s)]	Electron mobility
mup_P3HTPCBM	1e-6 [m ^ 2 / (V * s)]	Cavity mobility
N_c_P3HTPCBM	1e25 [1 / m ^ 3]	Navigation bar
epsilonr_P3HTPCBM	3.4	Relative forgiveness
a_P3HTPCBM	1.8 [nm]	The average distance traveled by the mean electron and hole
kf_P3HTPCBM	1.4e4 [1 / s]	Vap rate Ashi
gamma_P3HTPCBM	(e_const / (epsilonr_P3HTPCBM * epsilon0_const)) * (mun_P3HTPCBM + mup_P3HTPCBM)	Effective mobility of electrons and cavities
n_init_P3HTPCBM	sqrt (N_c_P3HTPCBM ^ 2) * exp (-e_const * E_gap_P3HTPCBM / (2 * k_B_const * T))	Thermodynamic equilibrium concentration

The thickness of the two PCPDTBT composites: PCBM and OC1C10PPV: PCBM was considered to be 120 nm, but for P3HT: PCBM this value was considered 100 nm, because the thickness of these composites is one of the factors that strongly resolves. Gaining cell efficiency is impressive. Also, in all experimental and simulation studies for all three composites, the thickness of the active layer did not exceed these values and, by definition of constant conditions, the parameters and properties of each material were equal to these values. (..)

In the next section, the variables (used to simplify the properties of the structural components when defining the model) are required. This simulation, as discussed in the previous section for cell modeling, is used as input variables to the software environment. They are added with mathematical language.

Table 4-6- Input variables for all three composites

Variable	**Formula**	**Definition**
F		Field intensity
b	Equation21	Bessel function argument
R	Equation22	Recombinant rate
k_diss	Equation23	Resolution rate
p	Equation24	Probability of electron - hole pair separation
f_kernel	Equation25	Normal distribution function
P_prob	Equation26	Probability of electron - hole pair separation with more than one separation distance distribution
alpha	**Equation27**	The amount of absorption
phi	Equation28	Metal Working Function
Generation	Equation29	Production function

According to the definitions of switch 0, 1, 2 the formulas associated with the fixed parameters of all three composites have been rewritten as follows, for greater software performance and error minimization as well as obtaining the absorption value and production function of all three composites. It should also be noted that switch 0,1,2 represents OC1C10PPV: PCBM and PCPDTBT: PCBM and P3HT: PCBM composites, respectively.

Table 4-7- Change the fixed parameters to obtain the production function and the amount of adsorption

Variable	Formula
gamma	gamma_P3HTPCBM * (switch == 2) + gamma_PCPDTBTPCBM * (switch == 1) + gamma_P3HTPCBM * (switch == 0)
a	a_PEHTPCBM * (switch == 2) + a_PCPDTBTPCBM * (switch == 1) + a_P3HTPCBM * (switch == 0)
kf	kf_P3HTPCBM * (switch == 2) + kf_PCPDTBTPCBM * (switch == 1) + kf_P3HTPCBM * (switch == 0)
k_Organic	k_P3HTPCBM (lambda) * (switch == 2) + k_PCPDTBTPCBM (lambda) * (switch == 1) + k_P3HTPCBM (lambda) * (switch == 0)
E_gap	E_gap_P3HTPCBM * (switch == 2) + E_gap_PCPDTBTPCBM * (switch == 1) + E_gap_P3HTPCBM * (switch == 0)
affinity	affinity_P3HTPCBM * (switch == 2) + affinity_PCPDTBTPCBM * (switch == 1) + affinity_P3HTPCBM * (switch == 0)
mu_n	mun_P3HTPCBM * (switch == 2) + mun_PCPDTBTPCBM * (switch == 1) + mun_P3HTPCBM * (switch == 0)
mu_p	mup_P3HTPCBM * (switch == 2) + mup_PCPDTBTPCBM * (switch == 1) + mup_P3HTPCBM * (switch == 0)
N_c	N_c_P3HTPCBM * (switch == 2) + N_c_PCPDTBTPCBM * (switch == 1) + N_c_P3HTPCBM * (switch == 0)
epsilon_r	epsilonr_P3HTPCBM * (switch == 2) + epsilonr_PCPDTBTPCBM * (switch == 1) + epsilonr_P3HTPCBM * (switch == 0)
n_init	n_init_P3HTPCBM * (switch == 2) + n_init_PCPDTBTPCBM * (switch == 1) + n_init_P3HTPCBM * (switch == 0)
Generation_tot	integrate (Generation_func (x, z), z, 300 [nm], 800 [nm]) / (800 [nm] -300 [nm])

The next step is to define the exact values of the solar spectrum, based on the wavelength and density of the radiation, as follows. As can be seen, the variation of the radiation density varies from 280 to 4000 nm, from 1.20 * 10-20 to 28.4172 w / m2, respectively. These changes represent the average solar radiation power that reaches the maximum input power density of Pin = 1000 w / m2 at the cell surface of the light source. Using this diagram for the sun under the conditions of AM 1.5 (air mass) light spectrum, this value is then used to calculate the efficiency.

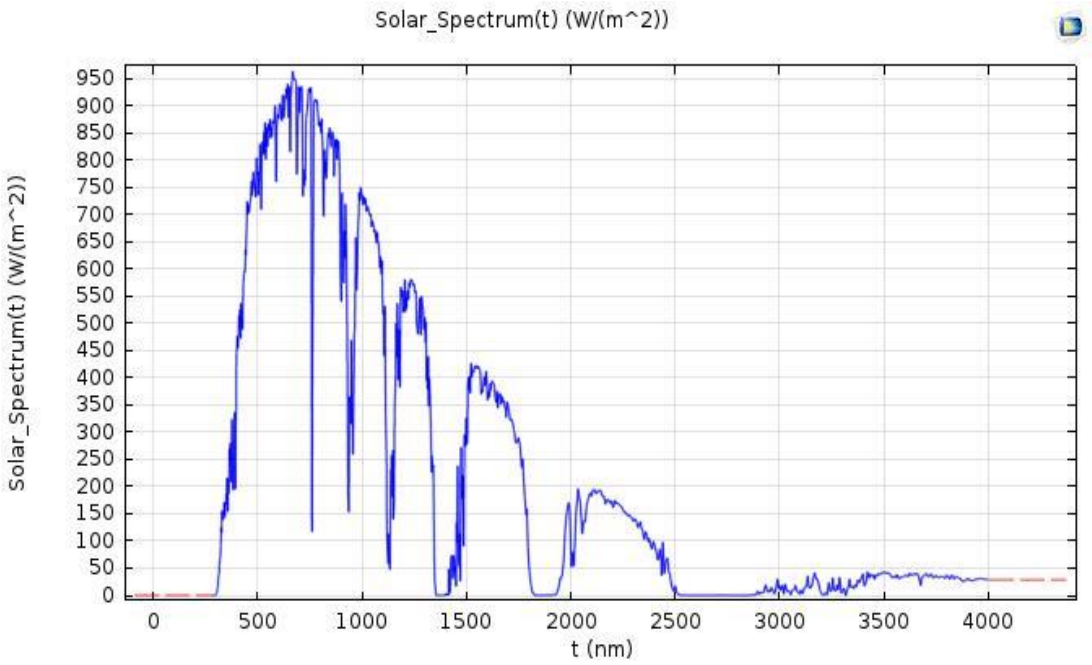

Diagram 4-1- Solar spectrum coming from the density of radiation and wavelength.

To obtain the refractive index of the OC1C10PPV: PCBM composite, we defined precisely the imaginary refractive index variations at wavelengths between 350-800 nm. The diagram obtained from this material shows us that the highest absorbance values are in the wavelength range of 400 to 500 nm.

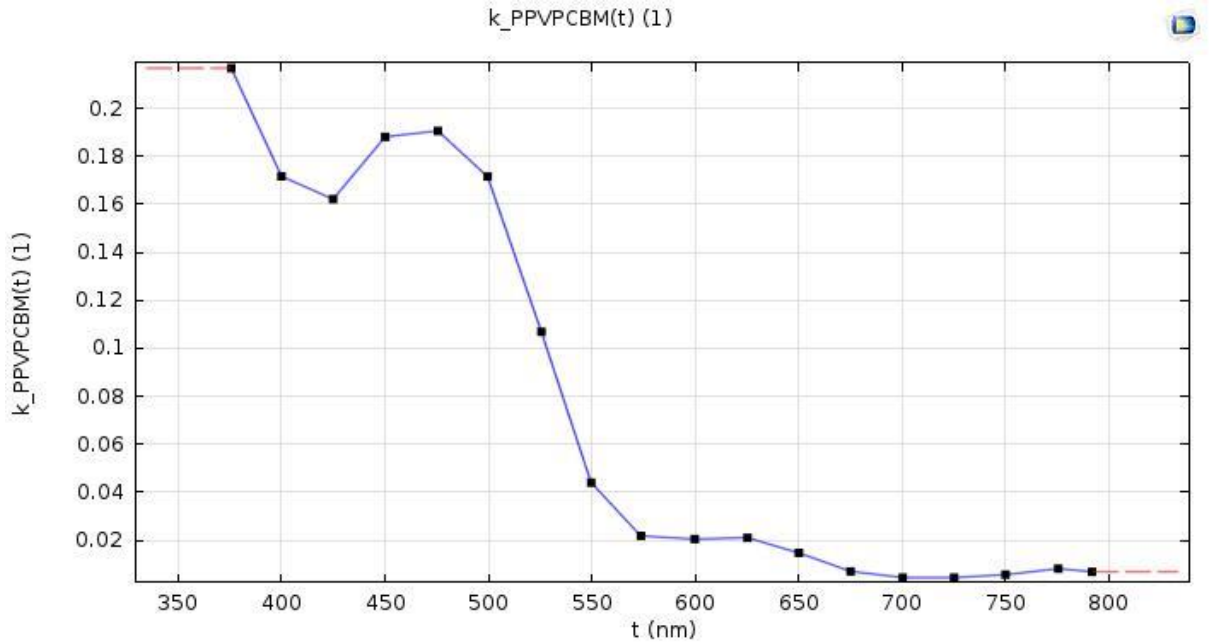

Diagram 4-2- OC1C10PPV Composite refractive index variations: PCBM based on imaginary refractive index and wavelength variations

To obtain the refractive index of PCPDTBT: PCBM also investigated the changes of imaginary refractive index in the wavelength range between 350-900nm. As it can be seen from the figure, the maximum absorbance is in the range of 800 nm in this material.

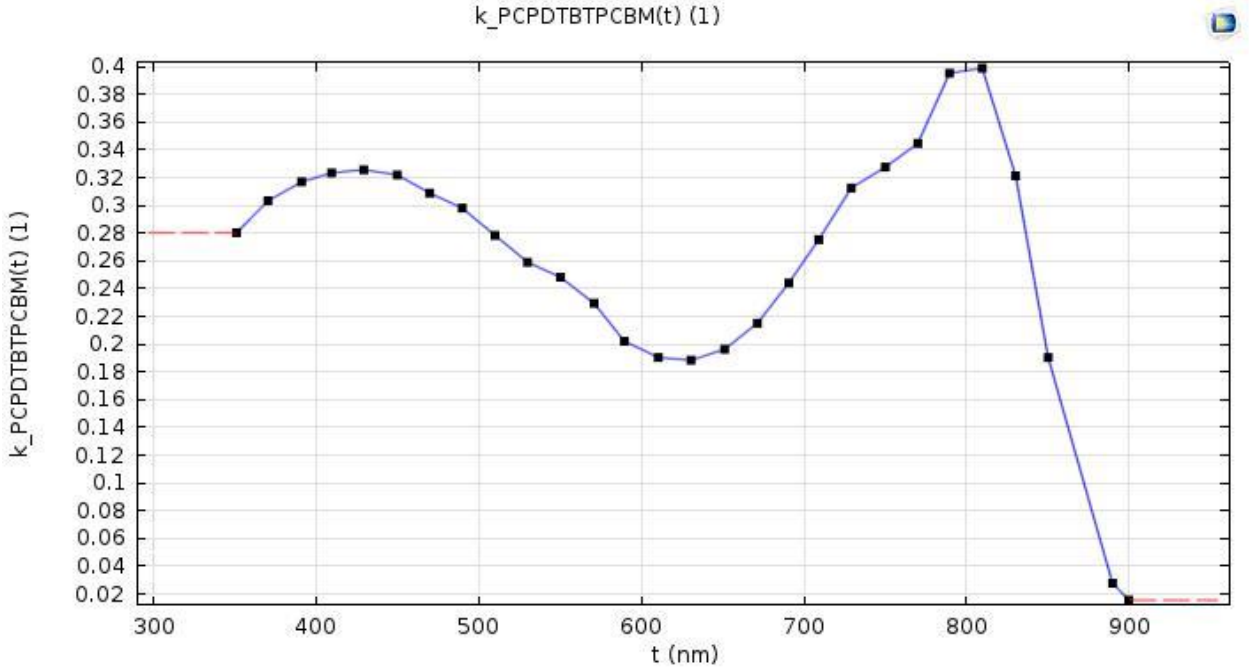

Figure 4-3- PCPDTBT composite refractive index variations: PCBM based on imaginary refractive index and wavelength changes

As before, the refractive index for P3HT: PCBM was obtained, which results from the figure being the maximum absorbance in the range of 500nm.

It is also important to note that the reason for using the imaginary refractive index-k in this study is to investigate the electrical properties of the organic solar cell. As a result, using this coefficient, only absorption is considered as the determining parameter for the investigation of these cells. It is also investigated to determine the optical properties of the cell from the refractive index n which has a spectrum different from that of the imaginary absorption coefficient.

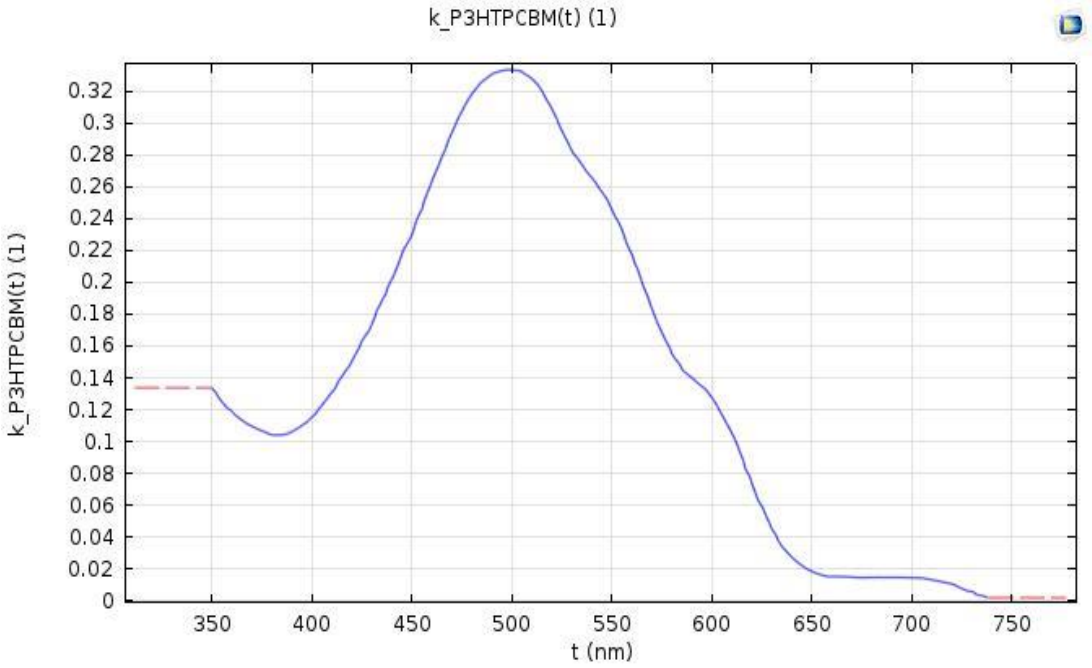

Figure 4-4- P3HT composite refractive index variations: PCBM based on imaginary refractive index and wavelength changes

To obtain the absorption function (exciton) for all three OC1C10PPV: PCBM, PCPDTBT: PCBM and P3HT: PCBM materials, we examined the absorption diagram in the wavelength range between 300-800 nm based on the switch 0-2. Equation 30:

$$\alpha = 4\pi k/\lambda$$

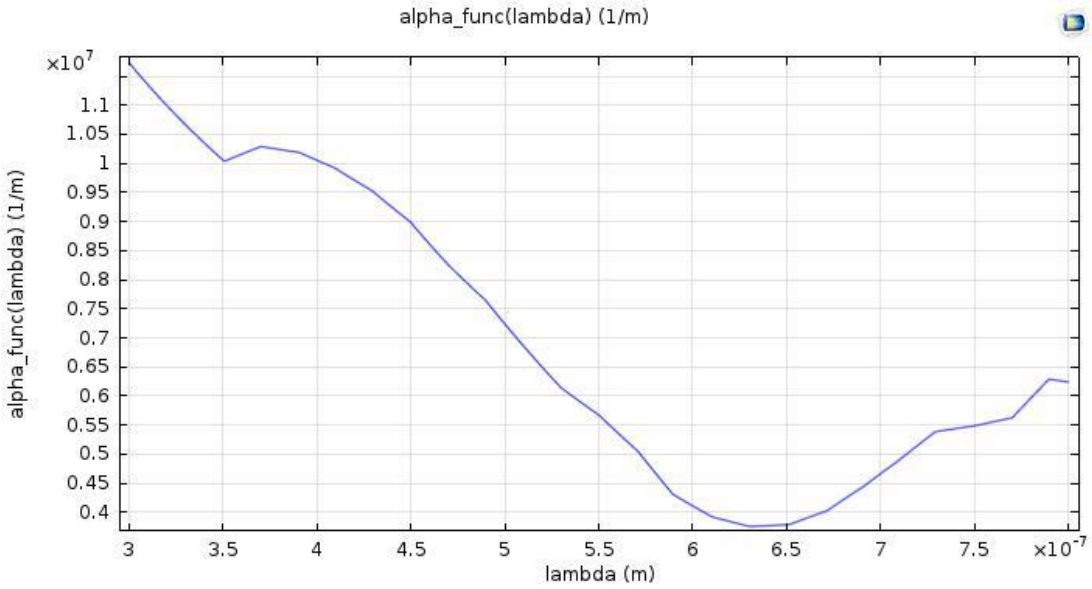

Figure 4-5- Chart of changes of absorption function in terms of wavelengths for all three composites studied

As can be seen, the maximum absorbance is in the wavelength range of 300 nm, indicating that up to 1.1 * 107 light can penetrate the material before being absorbed, causing the electrons to move to the energy bands as well as to conduction. Excitons into the donor / acceptor substrate.

Also the variations of the metal working function at wavelength are given by the following formula, Equation 31:

$$\boldsymbol{\varphi} = \frac{\lambda}{n\nu}$$

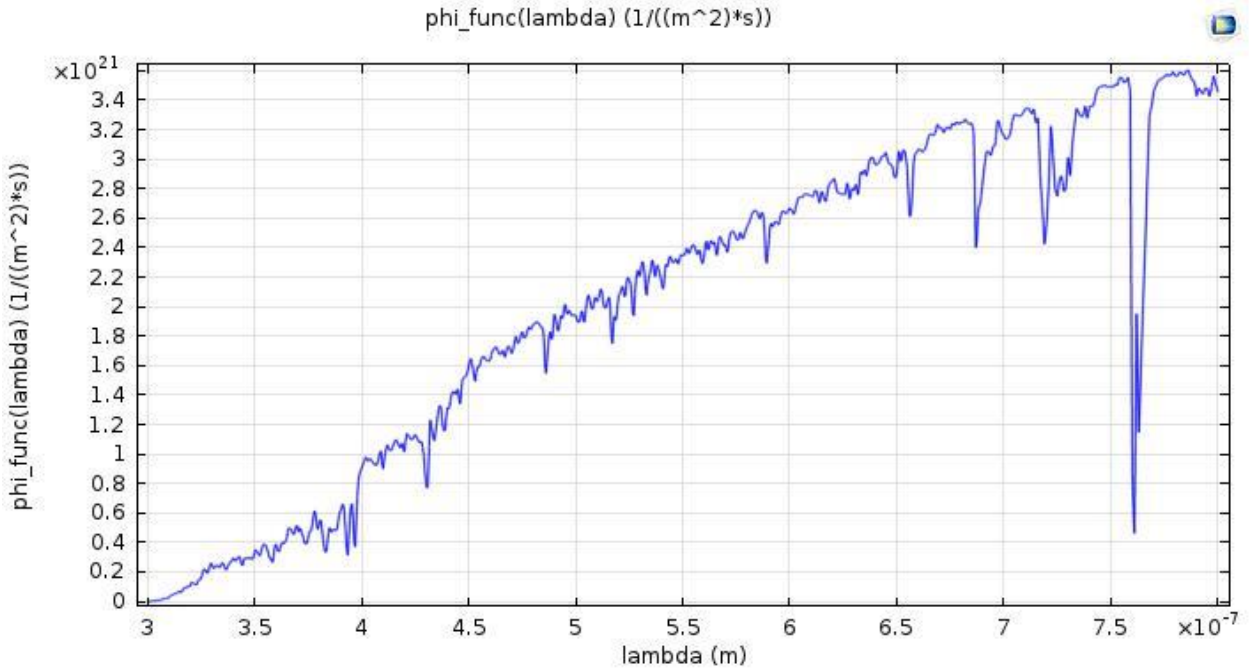

Figure 4-6- Wavelength changes of metal working function for all three composites

Finally, the production function is obtained by the following formula, Equation 32:

$$G = \alpha\varphi e^{-\alpha x}$$

In fact, this function is derived from the work and absorption functions in three dimensions which depend on the wavelength and the location.

In fact, the production function states at what wavelength and at what distance from the active layer, when the photon is absorbed, it has the highest rate of exciton production rather than recombination. Fig. 22 shows that at excitation wavelength 750 nm over 200 nm (outside the active layer range and near the anode) the highest exciton production occurs.

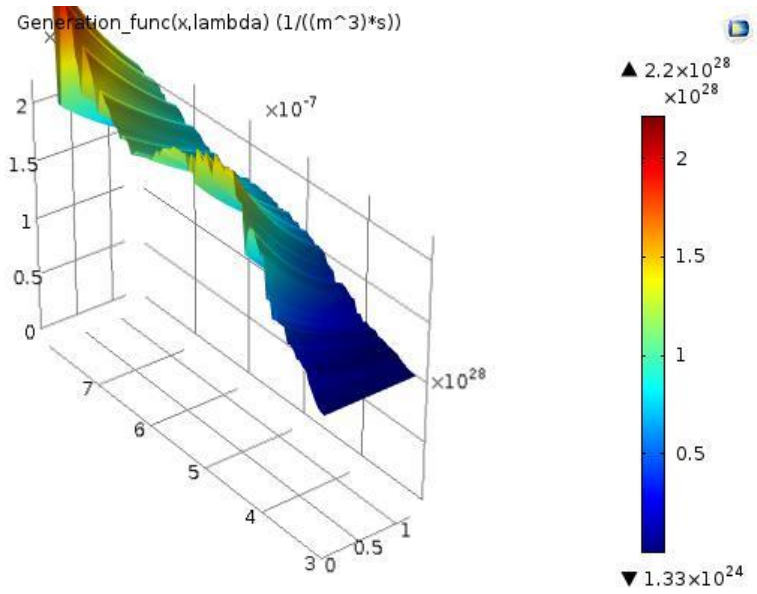

Figure 4-4- ؛ Diagram of wavelength and location-dependent production function for all three composites

The reason for studying these graphs is because of studying this cell in a specific spectrum (300–800 nm), which means that we did not restrict the cell to a specific wavelength and examined under AM 1.5 light conditions.

In the semiconductor section, taking into account the whole range of the definition of organic matter used in the active layer and the characterization of carrier statistics based on Maxwell-Boltzman rules and the solution based on electrons and holes (and not just The majority carriers) examined further the cell in question. The dependent variables in this section were the electrical potential and the electron and hole variables. The determinant relationships for the chosen domain are by default the model of semiconductor (organic) material as follows. In fact, rewriting and modifying the governing equations to determine boundary conditions in an organic solar cell were discussed below;

Poisson's Equation, Equation 33:

$$\nabla.(\varepsilon_r \nabla V) = q(n - p + N_A^- - N_D^+)$$

Electron and hole recombination rate, equation 34:

$$\frac{1}{q}\nabla.J_n = -U_n \text{ و } \frac{1}{q}\nabla.J_p = U_p$$

When both the diffusion current and the thrust current flow, there is an electric field as well as the carrier density gradient, so the overall electron and hole current density is as follows:

$$J_n = \left(\mu_n \nabla E_c + \frac{qD_{n,th}}{T_l} \nabla T_l\right) n + \mu_n k_B T_l G(nlN_c) \nabla \mathrm{n}$$

$$J_p = \left(\mu_p \nabla E_v - \frac{qD_{p,th}}{T_l} \nabla T_l\right) p - \mu_p k_B T_l G(plN_v) \nabla \mathrm{p}$$

The equations of energy for the capacitance band and conduction band are as follows, equation 35:

$$E_c = -q(V + \chi) \text{ و } E_v = -q(V + \chi + E_g)$$

Also, the electrical potential was assumed to be V = -4x (v / m).

In the selected range the recombination rates of electrons and holes were considered as follows:

$$R_n = R_{n,0} \text{ و } R_p = R_{p,0}$$

Also, the rate of electron and hole production in the selected range in the wavelength range between 300-800 nm is as follows:

$$G_n = G_{n,0} \text{ و } G_p = G_{p,0}$$

Boundary conditions are defined by default, taking into account equilibrium conditions and in the absence of electric current, as follows:

$$n.J_n = 0 \text{ و } n.J_p = 0 \text{ و } n.D = 0$$

Metal contacts (anodes and cathodes) on both sides of the organic matter are influential boundary conditions on the desired models which follow the following functions.

Scattering current for electrons and holes, equation 36:

$$J_n.n = -qv_n(n - n_0), \qquad J_p.n = qv_p(p - p_0),$$

Number of electrons in conduction band (carrier density), equation 37:

$$n_0 = N_c \exp\left(-\frac{\varphi_m - \chi}{k_B T_l}\right)$$

And the number of holes in the capacity bar, equation 38:

$$p_0 = N_v \exp\left(\frac{E_g - \varphi_m + \chi}{k_B T_l}\right)$$

Electrical potential, Equation 39:

$$V = -\varphi_m - \frac{1}{q}\Delta E_f + V_0$$

And finally, the amount of form energy that is roughly in the energy band gap, equation 40:

$$\Delta E_f = \frac{k_B}{2q}\left(Tln\left(\frac{N_v(T)}{N_c(T)}\right) - T_0 \ln\left(\frac{N_v(T_0)}{N_c(T_0)}\right)\right) + \chi^0(T_0) - \chi^0(T) + \frac{1}{2q}\left(E_g^0(T_0) - E_g^0(T)\right)$$

This is how they are calculated.

The type of anode and cathode contact is based on the Schottky contact. The recombinant surface velocities for the electrons and cavities corresponding to the ionic heat model were considered as vs, p = 19006 m / s, vs, n = 21605m / s, respectively. Also note that in this case the V0 anode voltage is equal to zero and for the cathode equal to the voltage applied to determine the boundary conditions. On the other hand, by considering boundary conditions in heterojunction and defining continuous quasi-Fermi levels continuity model, the following equations are defined:

$$E_{fn,1} = E_{fn,2}, E_{fp,1} = E_{fp,2}, D_1 = D_2$$

In the study area, in some cases during a structural simulation it is desirable to observe its role in the output by modifying or sweeping a parametric sweep. Here we study their role by sweeping the switch0, switch1 and switch 2 parameters and the voltage (whose range ranges from zero to one with a change rate of 0.01 and again by sweeping the said switches by changing the active layer thickness). we put.

Chapter Five
Results

Introduction

In this section, by considering parameters, variables and applying governing equations and appropriate boundary conditions for simulating organic solar cell in COMSOL software environment, succeeded in obtaining energy diagrams, carrier densities (electrons and holes), electrical potentials, variations We measured voltage-current and voltage-power, external quantum efficiency, and thickness changes of the active layer on the cells. Examination of each of these diagrams helps us to better understand the behavior of solar cells and a model of optimal performance.

Energy diagram

By applying the formulas mentioned in the preceding chapter, defining boundary conditions for bulk heterojunction ◌̣ OC1C10PPV: PCBM in one dimension and applying Maxwell-Boltzmann probability statistics over 1 square meter for said layer with interface continuation parameter parameter) with C□ equal to one, the Fermi energy diagram between the capacitance bar and the conductivity bar is as follows. The capacitance and conductivity bands can be applied to an electric field, showing the state in which the conductivity and capacitance bands are separated by the energy band gap. Spatial dependence can be introduced using the x-axis (active layer) to indicate the semiconductor position in this direction. If the electric field is not applied, the strips are merely horizontal lines. If a constant electric field is present, the energy bands must be tilted because of the constant gradient in the energy and the carriers will experience an F force of magnitude qε in the directions shown and to lower the potential energies. They move themselves.

The PN junction (corresponding to (OC1C10PPV): PCBM) represents a system of charged particles in equilibrium emission whose electrochemical potential is constant and independent of position. The electrochemical potential describes the average electron energy and is represented by Fermi energy. This means that under equilibrium conditions, the form balance has a fixed position on the PN bond band diagram.

(Fermi energy is an electrochemical potential of electrons in a material, in which case it represents the average energy of the electrons in the material.) ()

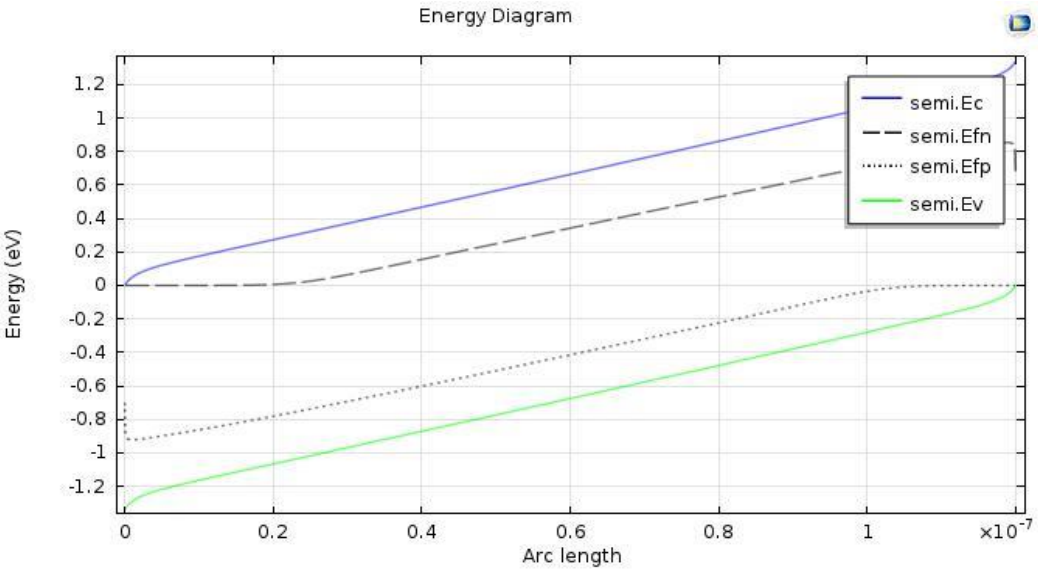

Chart 5-1 - OC1C10-PPV Energy Chart: PCBM is the blue line for the conduction band and the green line for the capacitance band and the dotted line is the electron and hole Fermi energy.

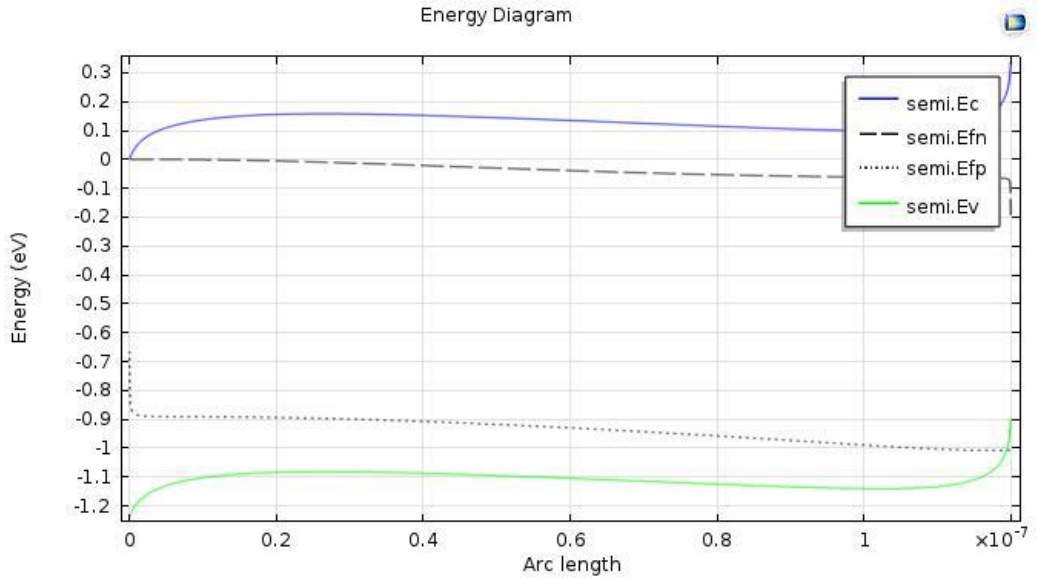

Figure 5-2- PCPDTBT Energy Chart: PCBM

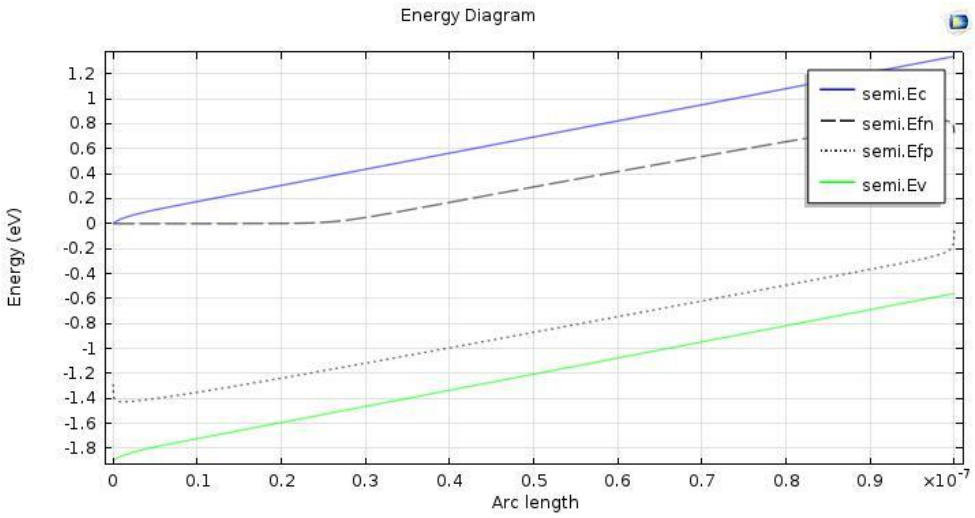

Figure 5-3- P3HT Energy Graph: PCBM

The above figure shows the band energy diagram of a PN junction of organic materials under equilibrium conditions. The distance between the Fermi surface and the capacitance band and - or the transmission band does not change in quasi-neutral regions such as isolated n-type and p-type semiconductors. Within the space-bar area, the conductivity and capacitance band are not represented by horizontal straight lines, in fact they are curved. This indicates the presence of an electric field in the area. Due to the electric field, a change in electrostatic potential has occurred between the boundaries of the space charge region. Throughout the discharge zone changes in carrier concentration are offset by changes in electrostatic potential. It is assumed here

That;

$n.J_p=0$, $n.J_n=0$

$V_1=V_2$, $J_n=J_p$

A potential step has emerged near the back contact that helps prevent the minority electrons from reaching the common surface of the active layer due to the back surface electric field created at the step location.

These graphs show that by varying the amounts of electron mobility and cavity mobility in different materials, a change in the Voc value is achieved and ultimately affects cell efficiency. As can be seen, in (OC1C10PPV): PCBM compared to PCPDTBT: PCBM, Voc decreased, thus reducing the efficiency (OC1C10PPV): PCBM cell also decreased compared to P3HT: PCBM and PCPDTBT: PCBM. Also, as shown in the diagrams for P3HT: PCBM is the Voc value and therefore some efficiency between the two materials.

5.3- Carrier density chart

Every action on semiconductor devices depends on the carriers that carry the load inside the semiconductor and cause electrical current. To determine or understand the performance of these devices, it is important to determine the exact amount of these load carriers.

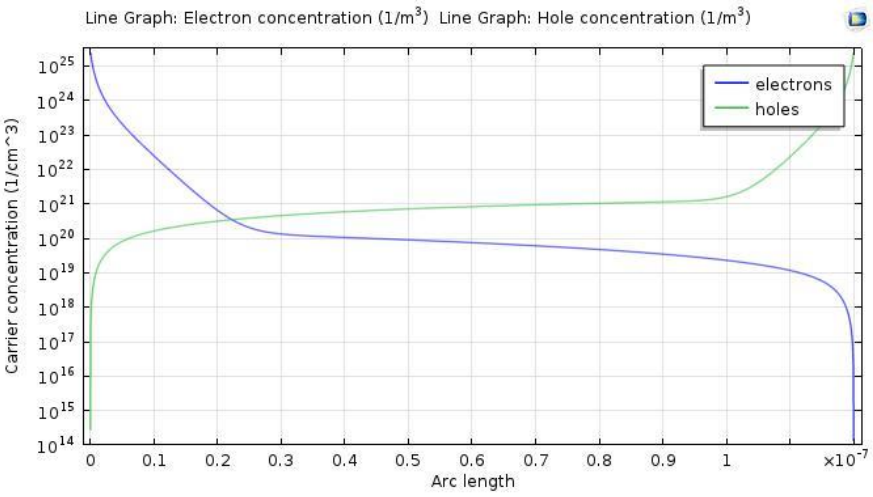

Figure 5-4- Carrier density chart for OC1C10PPV: PCBM. The blue lines correspond to the electron concentration and the green lines to the hole concentration.

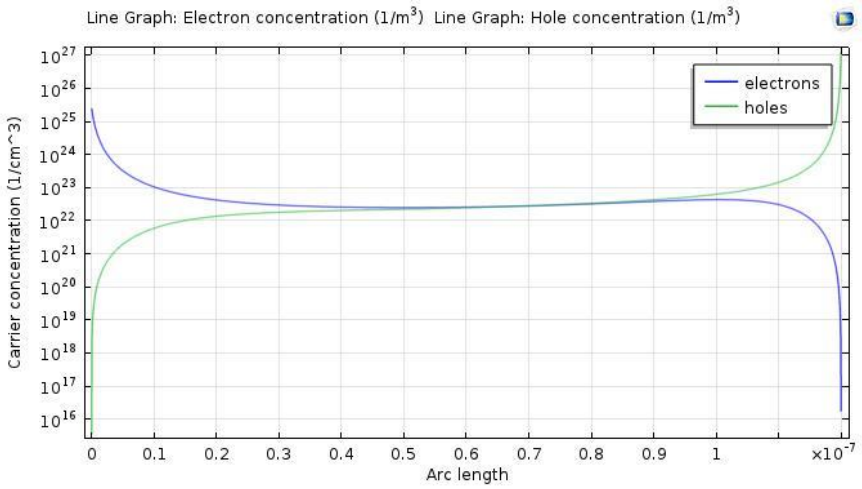

Figure 5.5- Carrier density for PCPDTBT: PCBM

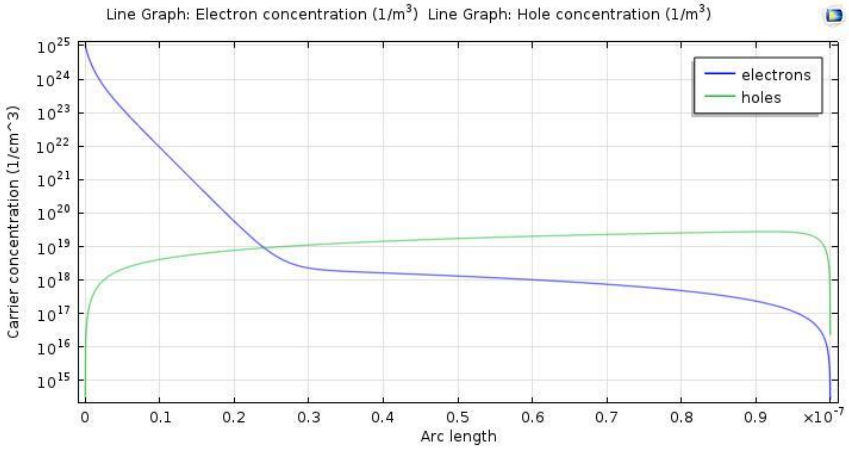

Figure 5-6- Carrier density chart for P3HT: PCBM

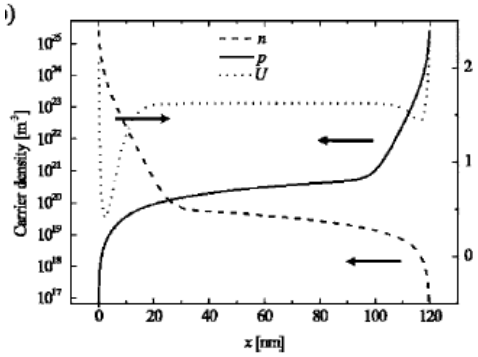

Figure 5-7- Carrier density chart for OC1C10PPV: PCBM in the experimental study

The concentration profile of the charge carriers in a p-n bond of the organic material of the active layer is presented above. In the quasi-neutral regions the electron and cavity concentrations are similar to the isolated doped semiconductors. In the space-charge region, the concentration of the carrier carriers of the majority is rapidly declining. This fact allows us to assume that the space-bar area is evacuated from moving cargo carriers. This assumption means that the load of mobile carriers represents a negligible share of the total space charge in the discharge area. The space charge in this region is completely determined by the ionized impurity atoms in the fixed lattice.

Also shown in this graph is the location of the collisions of the electron and hole carriers, which represents the Fermi energy range (hence, the VOC between the capacitance band and the conduction band. When the carrier concentration for OC1C10PPV: PCBM is 1 / cm3 10201.5 and PCPDTBT: PCBM is 1 / cm3 * 10221.2 and for P3HT: PCBM is 1 / cm3 * 10191.1 within the active layer energy range.In the case of OC1C10PPV: PCBM results obtained from COMSOL software correspond to experimental results.

As can be seen, the blue curve of the electron concentration and the green curve of the short circuit of the cavity in the active layer versus the distance between the anode and the cathode with electron mobility of 2.5 * 10-7m2 / Vs and cavity mobility of 3 * 10-8 m2 / Vs. is showing.

For PCPDTBT: PCBM also shows electron and hole concentration in short circuits with electron mobility of 3 * 10-7m2 / V.s and cavity mobility of 4.5 * 10-8m2 / V.s. As can be seen from Equation 12, a high increase in carrier density results in a high increase in carrier recombination. In the case of P3HT: PCBM, electron mobility of 10-5m2 / V.s and hole mobility of 10-6m2 / V.s are also considered.

Examination of these graphs shows that the highest efficiency of BHJ organic solar cells is controlled by the balance between mobility and concentration of carriers and recombination of charge carriers. Too much or too little mobility of the carriers results in a loss of efficiency in different organic solar cell mechanisms. Therefore, the optimum mobility of a carrier critical to obtain maximum solar cell efficiency must be completed and implemented ().

5.4- Electrical potential diagram

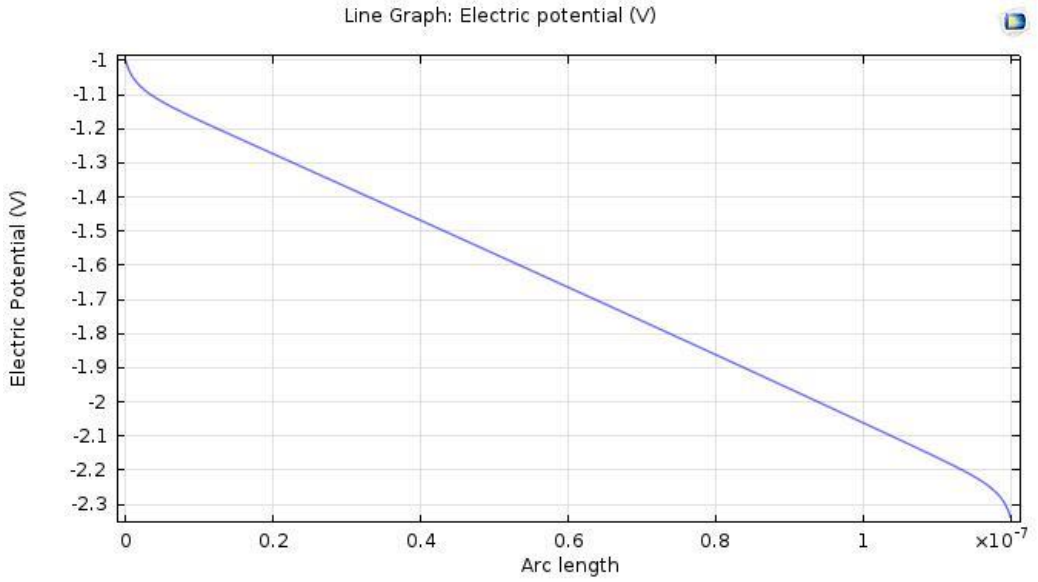

Figure 5-8: Electrical potential for OC1C10PPV: PCBM

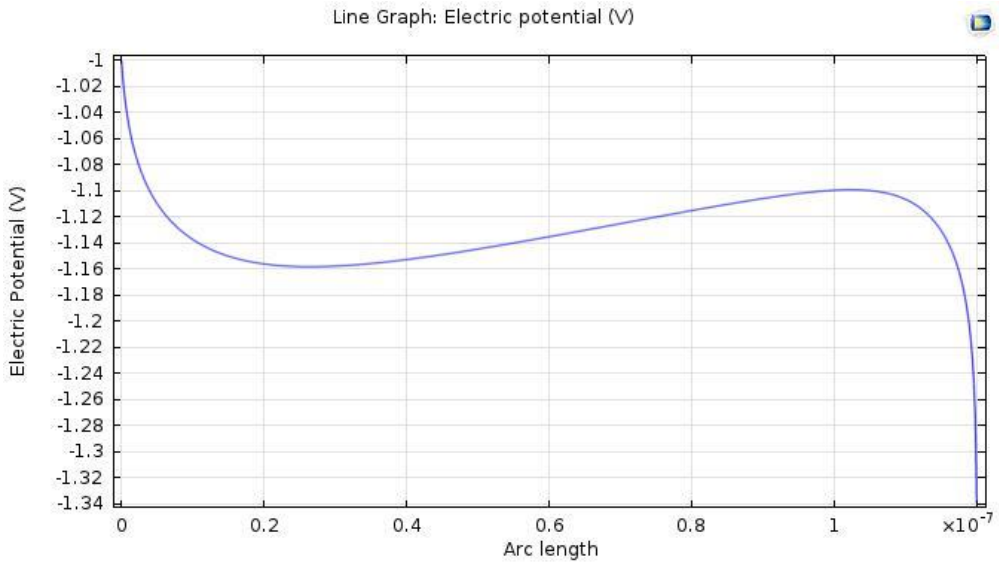

Figure 5-9- Electrical potential diagram for PCPDTBT: PCBM

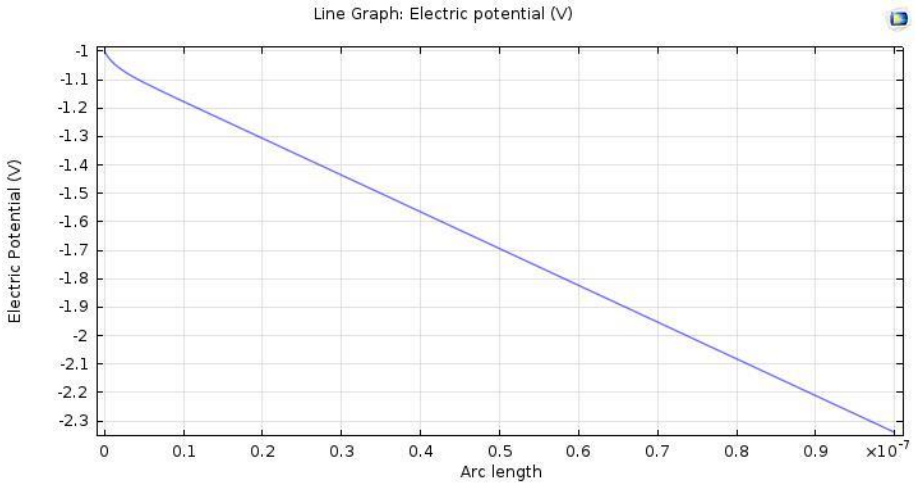

Figure 5-10- Electrical potential for P3HT: PCBM

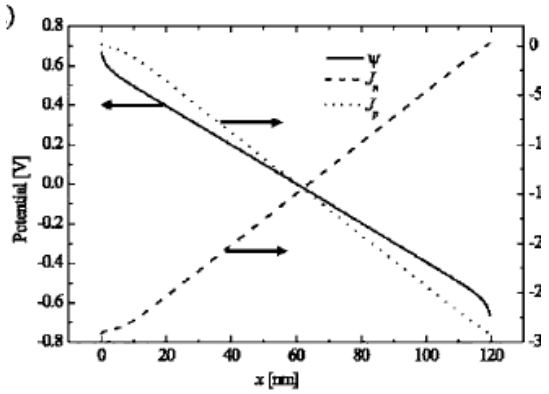

Figure 5-11- Electrical potential diagram for OC1C10PPV: PCBM in experimental study

As expected, the amount of potential along the active layer decreases. The potential for light irradiation is approximately equal to the potential for darkness (we did not show). While the ohmic contact does not inject bias into the bias, the carrier density at the contact is very high. The number of photogenerated loads is not sufficient to change the potential significantly. With the exception of the bending band near the contact resulting from a large amount of charge, the field inside the device is stationary and thus simultaneously equal to the dissociation rate. As a result, the current density shows a linear dependence on the position of the active layer in the device. The only exception is that near the contact where the density of both electrons and the hole is high, especially near the high contact X = 0, recombination becomes important.

Simply put, at X = 0, the active layer faces an increase in electrical potential due to the high density of the carriers resulting from the carriers' production and thus their recombination near the anode surface, and then due to the electrical current flowing between the anodes. And the cathode, and the movement of the carriers towards them, thereby reducing the density of the carriers, is associated with a decrease in the electrical potential.

The curvature zone is affected by the compound open rate. In low-injection barriers, high electric field prevents the distribution of minority charge carriers at the metal electrodes. Because in VOC conditions electrons and cavities must be transported simultaneously, the recombination at the electrode surface is minimized and the recombination of charge carriers mainly located in the bulk of the active layer. As the injection barrier increases, the bending area decreases or even reverses, with significant diffusion of minority and majority charge carriers into the anode and subsequent surface recombination. Since in the thermal equilibrium the rate of production must be equal to the recombination rate, the total recombination rate is constant. In the VOC the device is directly restricted by injection barriers.

The current densities are almost zero across the device. The reason that current density may not be zero everywhere depends on the field's dependence on the rate of production. In the case of fixed production rates, the current density will be zero everywhere. Therefore, with respect to the electric potential diagrams and the carrier concentrations, the densities are almost symmetric.

Diagram I-V and P-V

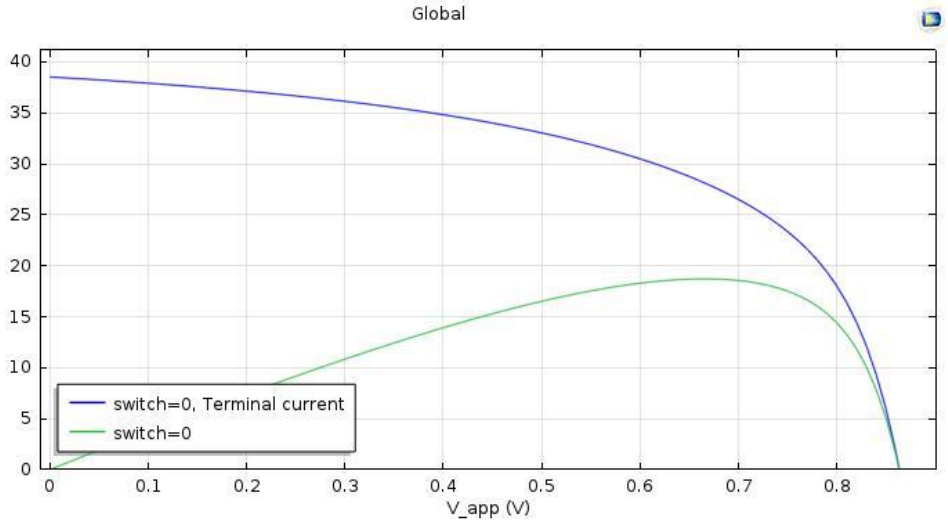

Figure 5-12- Flow Charts - Voltage and Voltage - Power for OC1C10PPV: PCBM. The blue lines associated with the P-V diagram and the green lines represent the I-V profile.

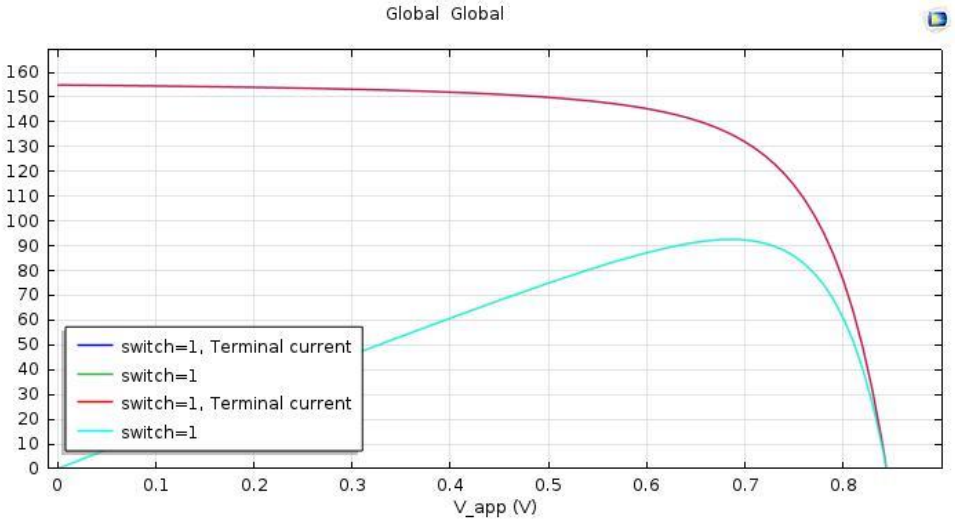

Graph 5-13- Voltage- Current and Voltage- Power Charts for PCPDTBT: PCBM

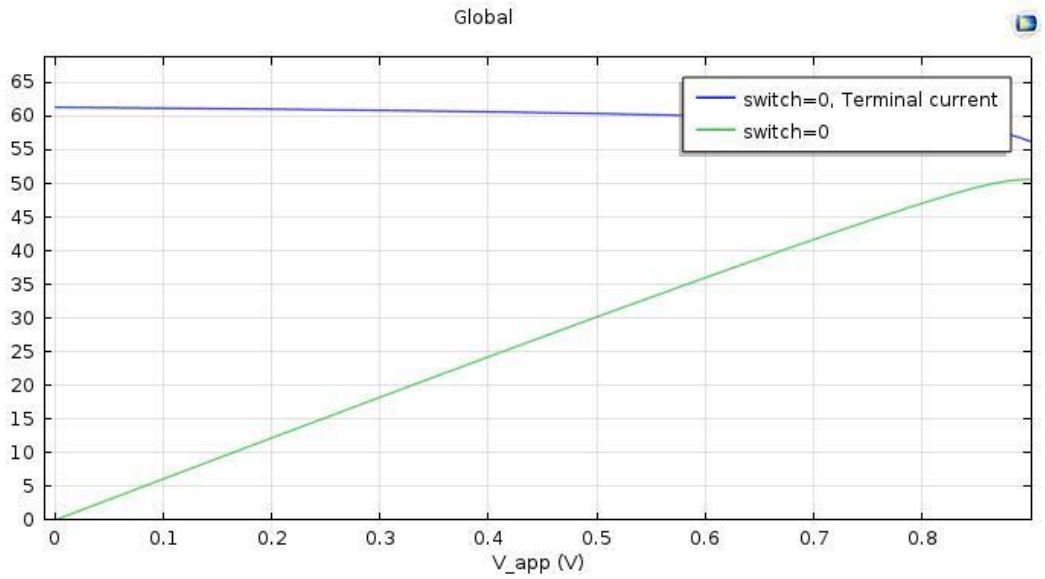

Figure 5-14- Voltage- current and voltage- power diagrams for P3HT: PCBM

This is a useful way to imagine solar cell performance: The p-n junction shows the voltage-current behavior itself. If the p-n junction is illuminated in the junction region, then in the inverse bias, the inverse current increases dramatically, due to the electron-hole pairs created by the illumination. Without optical generation, the available electrons and holes that form the inverse saturation current are carriers of the heat-producing minority with low density.

In direct bias, the inverse current still flows but is usually smaller than the broadcast current. However, in a solar cell, the current produced by light is much larger than the diffusion current and will be subject to the flow of current until the direct bias conditions are stronger. The solar cell I-V characteristic is shown in the figure above. A proportional operating point for the solar cell is shown in which the current flows through the outer orbit outside the positive terminal of the p-n junction (p side) then into the negative terminal (n side). The current flow at this point of operation is still recessive of the carrier-generated light drift, not the majority carrier propagation.

The efficiency or function of solar cells can be approximated by the voltage-current curve. In the absence of light, this piece acts like a diode but shifts when the curved light is vertical due to the current.

With the help of the I-V diagram we can obtain the FF and efficiency for the solar cell under study. Voltage diagrams were also analyzed.

FF is the ratio of the maximum power attainable to the output of the open circuit voltage and the short circuit current obtained by Equation 41;

$FF=P_{max}/V_{oc}*J_{sc}$

Solar cell efficiency is also obtained through Equation 42 by means of the I-V and P-V graphs.

$$\eta = \frac{J_{SC} \times V_{OC} \times FF}{P_{in}}$$

The results are listed in Table 9. Solar cell efficiency In the experimental study for solar cell with active layer OC1C10PPV: PCBM was 2.5% and our result in COMSOL environment was 2.765% with relative error rate of 9.42% which indicates the ability and It shows the accuracy of this software to simulate these cells.

Also in the case of P3HT: PCBM in various experimental experiments, this efficiency was calculated to be 5%, which corresponds to our simulation result and our assumption of considering the electron demand of this composite as one. It should be noted that the yield of this material in our simulation was 5.05% with a relative error of 0.99%, indicating that it is important to determine the initial parameters and assumptions to obtain its electrical properties correctly and accurately.

Table 5-1 - Table of the final results of the simulation

Organic active layer	V_{OC} v	J_{SC} A / m2	FF %	P_{max} w / m^2	η %
OC_1C_{10}-PPV: PCBM	0.86	38.5	0.56	18.71	2.76
P3HT: PCBM	1.5	61.3	0.55	50.59	5.05
PCPDTBT: PCBM	0.84	154.8	0.71	92.56	9.25

The above table shows that the PCPDTBT: PCBM yields 9.2% higher than the P3HT: PCBM and OC1C10PPV: PCBM simulations in the COMSOL simulation environment. It should be noted that the efficiency of these cells in the simulator environment is assumed to be based on voltage and wavelength changes and their temperature and electron demand constant. It is important to note that any of the energy and electron mobility parameters of the cavity can be altered by engineering the structure of the polymeric material itself, thereby altering the efficiency and other important output parameters of these cells. .

5.5 Diagrams of External Quantum Returns

The ratio of the number of charge carriers collected by a solar cell to the number of glowing energy photons given to a solar cell by landing photons.

The following diagrams show the values of external quantum yields that vary with wavelength. As it can be seen from this graph, in OC1C10PPV: PCBM composite the highest external quantum efficiency is related to the wavelength range of 300nm equal to 60.39%, in the P3HT: PCBM composite used in solar cell the highest value in the wavelength range. 500nm occurs which is 55.05%. It also has an approximate graphical representation of external quantum diagrams relative

to the other two graphs (ideally rectangular). In PCPDTBT matter: PCBM quantum yield change diagram shows interesting changes. As can be seen, the wavelength range of 300 nm has a maximum change for external quantum efficiency of 73.63% and then with a sharp external quantum decline at 650 nm (quantum efficiency of 35.76) and rising again. It shows this efficiency in the wavelength range above 800nm. This actually indicates that the wavelength of 650nm is minimal. All three of these graphs clearly state that the external quantum efficiency is related to the absorption coefficient graph.

Comparing the process diagrams of external wavelength quantum changes for OC1C10PPV: PCBM and PCPDTBT: PCBM and P3HT: PCBM materials at a typical 500nm wavelength has 44%, 55% and 56.5%, respectively.

Examination of these graphs actually shows us what spectrum of use of these materials as active layer in organic solar cells has the highest efficiency and performance. These diagrams are further explored for the design and fabrication of tandem solar cells, as they do not overlap active layers in the same spectrum and absorb a wider range of sunlight.

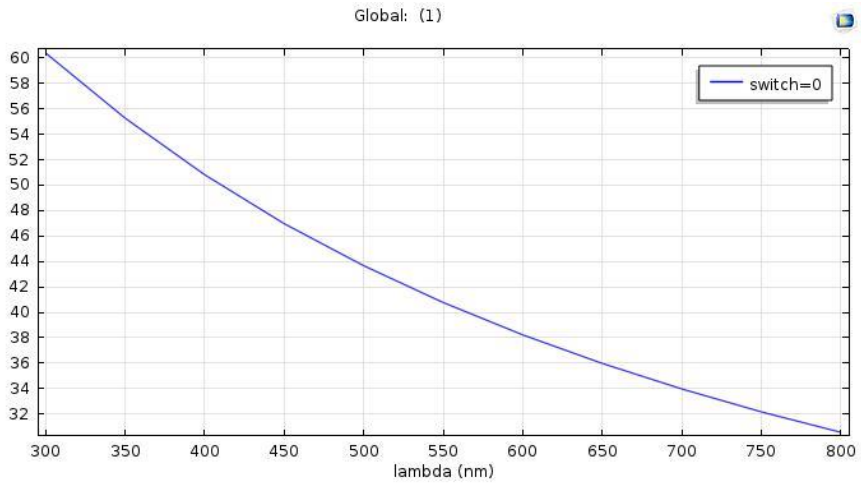

Diagram 5-15- External wavelength quantum efficiency variations for OC1C10PPV: PCBM

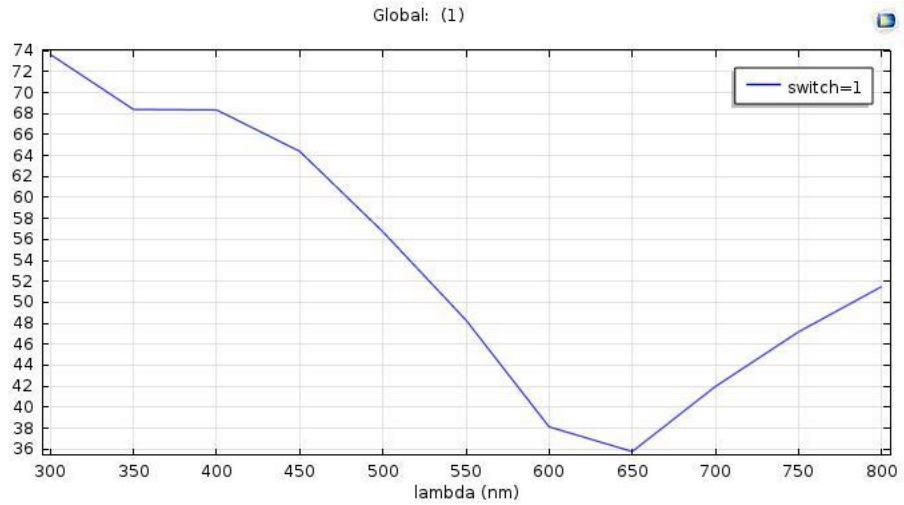

Diagram 16- External wavelength quantum efficiency changes for PCPDTBT: PCBM

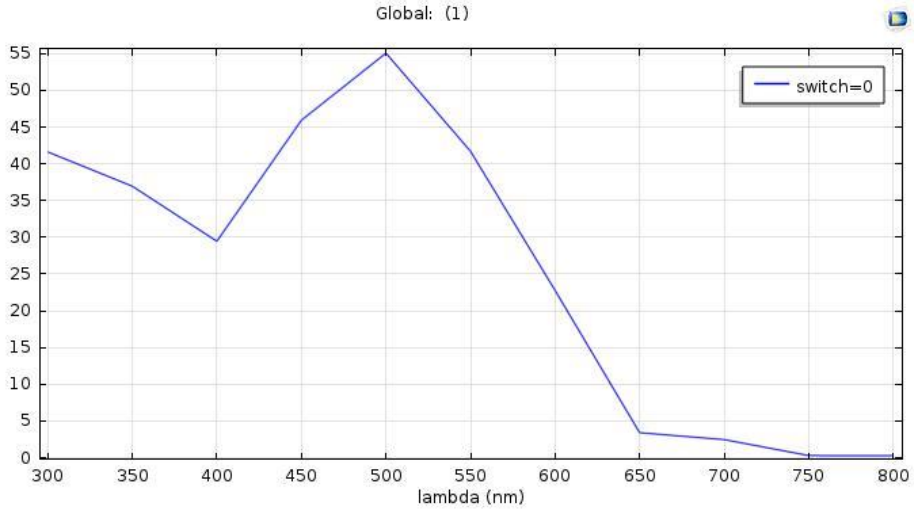

Figure 5-17 - External wavelength quantum efficiency change diagram for P3HT: PCBM

5-6- Investigation of the effect of thickness changes of active layer on flow in cells

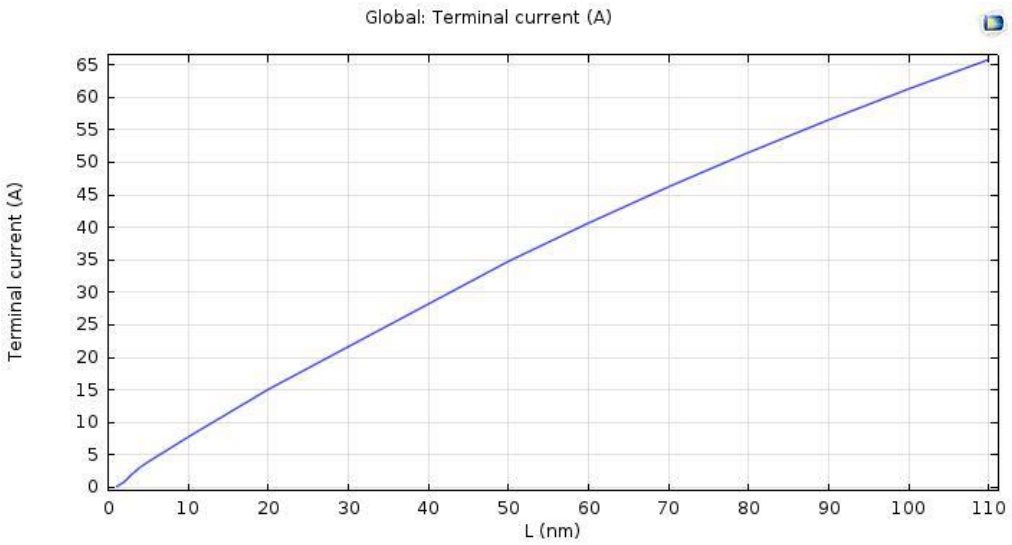

Figure 5-18- Flow on active layer thickness changes for P3HT: PCBM

The flow diagram changes according to the thickness changes of the active layer of OC1C10PPV: PCBM as shown in Figure 41. The thickness of this cell varied from 1 to 200 nm. It should be noted that the change trends were calculated once from 1 to 5 nm and then from 10 to 200 nm by eliminating the thicknesses of 30 and 40 nm, due to first-order Bessel function error.

In the case of PCPDTBT: PCBM was studied as before, with the trend of thickness changes with flow. The initial modifications of this material, such as OC1C10PPV: PCBM, were from 1 to 5 nm and the secondary changes from 10 to 130 nm were considered.

For the P3HT: PCBM material, initial changes were considered as well as secondary but secondary changes from 10 to 110 nm.

The remarkable point in all three results from these diagrams is that all three materials at thicknesses between 30 and 40 nm showed the Bessel function error in their diagrams. In this thick range it seems that the rate of production, dissociation and recombination of the excitons is strongly dependent on the thickness, thus decreasing the exciton emission length in the co-material andWe accept. It is also important to note that the thickness of the active layer should be proportional to the length of the excitons in this layer, and if the thickness of the layer is greater than the length of the excitons, the excitons will not have the energy required to reach the donor-acceptor interface. Was. Therefore, for the P3HT: PCBM material a maximum thickness of 110 nm and for PCPDTBT: PCBM a maximum thickness of 130 nm are achievable and higher thicknesses of these values prevent excitons from reaching the donor and acceptor segments in these composites.

In addition, the graphs of these materials show that the short-circuit current fluctuations are strongly dependent on the changes in the thickness of the active layer and the material of the material in the organic solar cell. So that the highest flow rate changes respectively PCPDTBT: PCBM and then P3HT: PCBM and finally OC1C10PPV: PCBM which affect cell efficiency. Therefore, it is expected that with respect to the result and also the production function changes,

the cell yields for OC1C10PPV: PCBM at 200nm thick and for P3HT: PCBM and PCPDTBT: PCBM will increase at 110nm and 130nm, respectively.

As noted, the highest flow rate thickness changes for active layers were due to PCPDTBT: PCBM material. If we discuss the three software diagrams at 100nm thick, we conclude that the flow rates in the OC1C10PPV: PCBM, P3HT: PCBM and PCPDTBT: PCBM composites have values of 34 A / m2, 61 A / m2, respectively. And 138 A / m2 indicating the performance of PCPDTBT: PCBM composite as an active layer in solar cells. It should be noted that the solar cell has a direct relation to the efficiency of the cell.

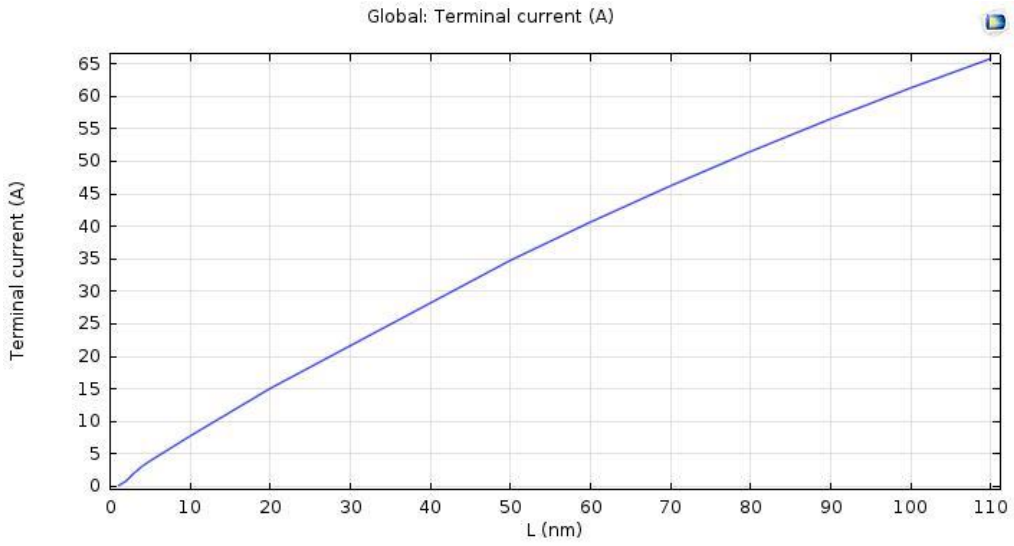

Chart 5-19 - Flowchart on Active Layer Thickness Changes for OC1C10PPV: PCBM

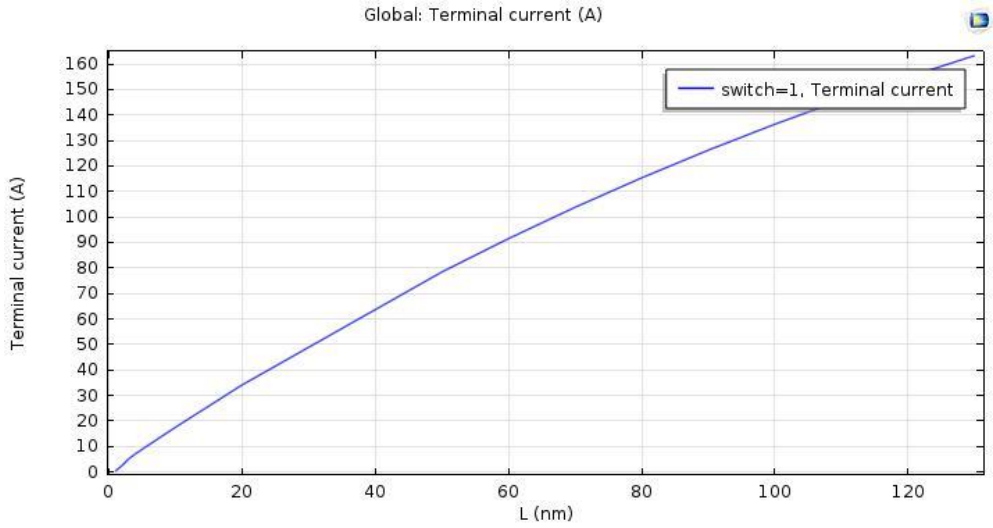

Figure 5-20 - Flow on Active Layer Thickness Changes for PCPDTBT: PCBM

Chapter Six
Conclusions and Suggestions

Conclusion

Considering the material diagrams of OC1C10PPV: PCBM, PCPDTBT: PCBM and P3HT: PCBM outputs of open circuit voltage, short-circuit current, FF and external power quantum efficiency and quantum efficiency, as well as the effect of organic layer thickness changes on current Short-circuiting with the help of COMSOL multiphysics software was investigated in organic solar cells and it was concluded that this software has the necessary and sufficient potential to predict the efficiency of these cells.

In this study, given all the parameters required for the simulation to be unavailable, assuming some parameters here the PCPDTBT: PCBM and P3HT: PCBM composite electron demand was considered to be equal to one (for OC1C10PPV: PCBM during past research). Equivalent to one proof) as well as keeping the temperature constant which greatly affects the open circuit voltage and short circuit current and thus the efficiency, by trial and error trying to match the simulation results with the experimental results for OC1C10PPV: PCBM It performed well and then PCPDTBT: PCBM and P3HT: PCBM simulations were performed correctly. As a result, it was found that the efficiency of OC1C10PPV: PCBM, which was 2.5% in laboratory investigations under AM1.5, was 2.7% in the simulation with COMSOL software. In addition, for the P3HT: PCBM material in vitro the yield was higher than 5% and in our simulation the yield for this material was 5.05%. In the case of PCPDTBT: PCBM composite, the yield was 9.2%.

Since the thickness of the active layer is one of several factors affecting the efficiency of organic solar cells by keeping the thickness constant in the initial simulation for OC1C10PPV: PCBM and PCPDTBT: PCBM (L = 120 nm), cell efficiency was well predicted but For P3HT: PCBM this thickness was reduced to 100 nm as the Bessel functions became difficult for the field-function resolution rate.

External quantum efficiency variations were also modeled well in the research based on wavelength variations. As can be seen, all three of these materials have the highest quantum yields in the specific spectrum, with the highest external quantum values respectively PCPDTBT: PCBM then P3HT: PCBM and finally OC1C10PPV: PCBM at wavelengths. Above 800, 500 and 300 nm.

In the case of flux changes with active layer thickness changes it was observed that the rate of flux changes was expected to depend on the thickness of the active layer. It was also observed that these flow changes are strongly dependent on the material, such that for OC1C10PPV: PCBM these changes up to 200nm thick but for PCPDTBT: PCBM and P3HT: PCBM up to 130nm and 110nm thick, respectively It is measurable. These changes help us find the optimal thickness and the right material to increase cell function.

6.2- Suggestions

• Study of organic solar cells by changing temperature, frequency and area parameters using COMSOL software

• Investigate the effect of changing the parameters of the active ingredient organic material on cell performance and efficiency separately such as electron demand, binding energy, thermodynamic equilibrium concentration, electron mobility and cavity and finally energy bandwidth with the mentioned software

• Modification of anode and cathode materials as well as modification of junctions and their effect on cell function

• Study and study to simulate tandem cells using these composites due to the lack of overlap of the absorption spectrum of these materials with the aforementioned software and thus maximum sunlight absorption.

• Study and study the optical properties of these cells with the mentioned software and compare with experimental research to validate this software to solve problems in optical properties

References

1. Zhou, Y. Bulk-heterojunction Hybrid Solar Cells Based on Colloidal CdSe Quantum Dots and Conjugated Polymers
2. Stella, M. Study of Organic Semiconductors for Device Applications
3. Krebs, F. C. Polymer Photovoltaics a Practical Approach
4. Janssen, R. A.; Hummelen, J. C.; Sariciftci, N. S.
5. Tarkuc, S. Tuning the Optoelectronic Properties of Conjugated Polymers via Donor-Acceptor-Donor Architectures
6. Thomas, C. A. Donor-Acceptor Methods for Band Gap Reduction In Conjugated Polymers
7. Thomas Kietzke "Recent Advances in Organic Solar Cells"
8. Brabec, C. J.; Sariciftci, N. S.; Hummelen, J. C.
9. Hadziioannou, G.; Hutten P.F.V. Semiconducting Polymers
10. Liao, K. S.; Yambem, S. D.; Haldar, A.; Alley, N. J
11. Gunes, S.; Neugebauer, H.; Sariciftci, N. S.
12. Thompson, B. C.; Frechet, J. M. J. Angew.Chem.
13. .Brabec,C.; Zerza, G.; Cerullo, G.; De Silvestri, S.; Luzatti, S.; Hummelen, J.C.
14. Cai, W.; Gong, X.; Cao, Y.
15. Mozer, A. J. Charge Transport and Recombination in Bulk Heterojunction Plastic Solar Cells.
16. Kalita,G.; Wakita,K.; Umeno,M. "Investigation of Nanostructured Organic Solar Cells with Transmission Electron Microscopy" Microscopy
17. Chiang, C; Fincher, C; Park, W; Heeger, A. Electrical conductivity in doped Polyacetylene
18. C. W. Tang. Two layer organic photovoltaic cell
19. A. Gregg, B. The Photoconversion Mechanism of Excitonic Solar Cells
20. Peumans, P; Uchida, S; R. Forrest, S. Efficient bulk heterojunction photovoltaic cells using small molecular-weight organic thin films
21. Hadipour, A; Boer, B; W. M. Blom, P. Organic Tandem and Multi-Junction Solar Cells
22. Zhong , Y; Tada , A; Izawa , S; Hashimoto , K; Tajima. Enhancement of *V* OC without Loss of *J* C in Organic Solar Cells by Modifi cation of Donor/Acceptor Interfaces

23. Min, J ; N. Luponosov, Yuriy ; Gerl , A; S. Polinskaya , M; M. Peregudova , S; V. Dmitryakov , Petr; V. Bakirov , A; A. Shcherbina , M; i N. Chvalun , S; Grigorian , S; Kaush-Busies , Nina; A. Ponomarenko, S ; Ameri , T; J. Brabec, C . Alkyl Chain Engineering of Solution-ProcessableStar-Shaped Molecules for High-Performance Organic Solar Cells
24. R. Forrest, S. The Limits to Organic Photovoltaic Cell Efficiency
25. Esiner, S; Bus, T; M. Wienk, M; Hermans, H; J. Janssen, R. Quantification and Validation of the Efficiency Enhancement Reached by Application of a Retroreflective Light Trapping Texture on a Polymer Solar Cell
26. SUNA.ir
27. Solar Cell Fundamentals by Adrienne Keita